Upscaling on Fracture Flow Models

Master of Science Thesis
in Reservoir Mechanics

Martin Sandanger Dugstad

Department of Physics and Technology
University of Bergen

June 1, 2017

Acknowledgements

I would like to most warmly thank my supervisor Kundan Kumar for the excellent guidance he have graciously given me. I have much appreciated all the time he spent helping me and how his door was always open. I would also like to thank my second supervisor Alessio Fumagalli for our informative discussions and for his help.

My thanks also goes to family and friends, especially to the lunch group for nice discussions on both our master thesis's and everything else.

Abstract

Fractures have a great impact on the quality of a porous media. The understanding of the fractures is important to describe the challenges linked to flow of geothermal heat, the transport of groundwater or transport of hydrocarbons in a porous media. The understanding of fracture can help to increase the energy production, or the extraction of clean drinkable groundwater. In this study we will investigate the effects of fractures in a porous medium by incorporate fractures as a lower dimensional geometric objects embedded in the porous matrix. Our approach here is to consider the fracture permeability as a diagonal tensor with the permeabilities scaled as an exponent of the width of the fracture. This thesis provides a rigorous approach towards *derivation of upscaled model* in a fracture. The quality of upscaling is further illustrated through extensive numerical examples that have been studied.

Contents

Chapter 1

Introduction and Motivation

1.1 Introduction

Porous media research has been one of the most active areas of research for the past century. This is not surprising considering that most of the material that we deal with is hardly impermeable. Porous media applications are ubiquitous in nature ranging from the fuel cell, petroleum related, water purification to biological applications such as brains, bones, and tissues. In particular, the energy and environment applications concern themselves with the porous media. The petroleum related applications such as extraction of hydrocarbons is essentially a study of the flow and transport processes in porous media. The water contamination in the ground water and the spreading of these contaminants are again the problems of similar porous media. In addition to these traditional applications, the big questions of climate science, the sea ice melting, the permafrost behaviour are all applications of porous media.

In the last century, there has been a tremendous research in the flow processes in porous media. The need for research in a porous medium is natural because of the inherent complexities involved. A porous medium consists of a solid skeleton surrounded by a void space such as soil. The void allows the flow to take place through this medium however the solid skeleton leads to obstruction in a freely flowing behaviour. There are inherent complexities in modelling the flow and transport behaviour in a porous medium. The geometry is quite complex with the pore space having a complex pattern. The properties of a typical porous medium are quite heterogeneous with the medium consisting of several constituents. With advent in the computational techniques, it has been possible to simulate the processes occurring inside such a complex medium. However, to have good results, we need to have appropriate models.

This thesis concerns with the effects of fractures in a porous medium. For accurate simulations it is important that the model describes the physical challenges in the best way as possible. Structures such as fractures needs to be taken into consideration, and they need to be described appropriately. This thesis derives appropriate models that incorporate the fractures in a porous medium.

1.2 Background of the problem

A fracture is a thin but long domain embedded in a porous matrix and characterise the heterogeneities in a porous medium. The flow and transport properties such as permeabilities may be drastically different from the porous matrix. At the same time, small width to length ratio makes it difficult that these properties are resolved explicitly through numerical methods. For these reasons, how to incorporate the fractures for flow computations in a porous medium remains a problem of outstanding interest. The influence of these fractures on the flow behaviour is quite strong. For instance, if there is a fracture network, the entire flow may simply take place through the fractures only. Incorporating fractures in a porous medium however raises

several interesting mathematical and engineering questions. In the next chapter, we provide a brief overview of this otherwise rich field of study.

The fractures appear in a porous medium in several sizes and shapes. There are three possibilities regarding incorporating them in the flow model. First, to resolve them fully by considering them as equidimensional domain as the porous medium. This would take into account the small width of the fracture. Secondly, we can consider the fractures to be a lower dimensional geometric object embedded in the porous matrix. This will imply that the model equations are defined in heterogenous domains with partial differential equations defined on both porous matrix as well as on the surface of the fracture. Thirdly, we can simplify the impact of the fracture by incorporating their effect only through their impact on the permeability of the grid cells. In the next chapter, we provide a brief overview of these approaches, and their extensions.

This thesis is concerned with the second approach: to incorporate fractures as a lower dimensional geometric objects embedded in the porous matrix.

Incorporating the fractures as lower dimensional geometric objects achieves two things: one, we do not need to resolve the fractures through a fine meshing. And secondly, we explicitly include the effect of the fractures. Resolving the fractures explicitly as a equidimensional geometric object implies unacceptably high computational costs. The typical fracture width is in order of 10^-3 m whereas a typical porous medium could be in orders of 100s of meters. Having a grid size that resolves the fractures completely immediately becomes an extremely expensive computational task. Moreover, we are not interested in the details of the pressure behaviour in the thin width of the fractures. Resolving therefore the fractures with a small grid cell does not provide any additional benefits as long as the overall flow pattern is concerned. On the other hand, including the effects of fractures through suitably altering the permeability of a grid cell is definitely the simplest and the cheapest approach. But this is bound to lead to unacceptable loss of accuracy in cases when the fractures are larger in length to be covered by one grid cell. In the cases when the fractures are long and covered by several grid cells, changing the permeability alters the property of all these grid cells and the flow behaviour would be significantly different from the reference solution. Our approach therefore covers a middle ground: considering the fractures as a lower dimensional object (hence, a 2D surface in a 3D porous medium geometry) with a partial differential equation on the surface coupled to the 3D geometry.

We assume that the fracture crosses the entire domain which simplifies the technical analysis. We consider a 2D rectangular geometry with the fracture in the middle. **The flow model to be used on a fracture surface depends on the permeability of the fracture!** An intuitive argument for the importance of the fracture permeability in deciding the type of flow model that should be used on the fracture surface is easy to follow. If the fracture permeability is extremely low then the fracture acts as a barrier and essentially leads to a breakdown in any communication of pressure between the two sides. In this case, the fracture therefore simply decouples the two subdomains. On the other hand, for the case when the fracture has high permeability, there would be no pressure difference along the vertical direction of the fracture. Thus, it would be natural a define a flow model on the fracture surface that is coupled to the porous matrix.

Our approach here is to consider the fracture permeability as a diagonal tensor with the permeabilities scaled as an exponent of the width. The permeability tensor inside the fracture is taken as:

$$K_f = \begin{bmatrix} \epsilon^\alpha & 0 \\ 0 & \epsilon^\beta \end{bmatrix}. \tag{1.1}$$

Considering the permeability tensor based on the width of the fracture seems strange at the first instance. There is no reason why the fracture permeability is dependent on the fracture width.

However, this should be interpreted as follows: let us say, we are given the permeability of the fracture. The question is what should be the average model that we should use for the fracture. The answer to this question depends on the scale of the permeability compared to the width of the fracture. We can therefore *determine the scale α and β* for the fracture permeability. Once, α and β are known, we can then determine the appropriate flow model to be used for the fracture surface.

Our approach is therefore to consider upscaled models for different scalings given by α and β. The upscaled models are obtained by taking the limit ϵ tending to zero. This is a mathematical limit and in practice this ϵ always remain a positive number. However, the idea is that *the upscaled model is the mathematical limit obtained by this procedure of ϵ tending to zero*.

Our approach borrows heavily from the work in (Chen, Pond, & Wang, 2012) where the authors have obtained equivalent boundary conditions for a heat insulation problem. However, for the fractures, such approaches have not been used before. The closest to our work in this thesis is the PhD thesis of Xavier Tunc (TUNC, 2012) where they have tackled the same problems. However, our approach is different from the approach they have used. We have performed the numerical computations for the upscaled models for different values of the parameter α, β and compared the quality of upscaling. Such sensitivity studies are not performed there. Also, we borrow ideas in the use of homogenisation techniques for deriving upscaled models including for thin layers as described in (Neuss-Radu & Jäger, 2007; Kumar, Neuss-Radu, & Pop, 2016; Kumar, Van Noorden, & Pop, 2011; Kumar, van Noorden, & Pop, 2014).

An exhaustive survey of literature dealing with fractures is quite ambitious and we refer to excellent textbooks (Bear, 1988; Helmig et al., 1997; Adler, Thovert, & Mourzenko, 2012) for some of the discussions. The fracture flow models treating the fractures as surfaces have been used in several papers including (Bastian et al., 2000; Singh et al., 2014; Girault, Kumar, & Wheeler, 2016; Reichenberger, Jakobs, Bastian, & Helmig, 2006; Fumagalli & Scotti, 2013; Formaggia, Fumagalli, Scotti, & Ruffo, 2014; Bukac, Yotov, & Zunino, 2016; Bukač, Yotov, & Zunino, 2015).

1.3 Contributions from this thesis

This thesis provides a rigorous approach towards *derivation of upscaled model* in a fracture. The quality of upscaling is further illustrated through extensive numerical examples that have been studied. The particular contributions in this thesis are enlisted below.

1. The derivation of the upscaled model through dimensional reduction in both 1D and 2D using a weak formulation and a dual problem to estimate the flux is a novelty. It outlines a new approach for deriving upscaled models for a fractured medium.

2. In 2D geometry, outlining the role of boundary conditions in deriving the upscaled model and the study of the quality of upscaling are also new. In particular, our numerical computations reveal that in the absence of periodic boundary conditions, the flow profile inside the fracture may become quite complex and develop boundary layers. Discussion on the continuity of the upscaled models with respect to the parameters α, β is also new.

3. Extensive numerical computations for the upscaled model and resolving the full ϵ model have been performed. This has provided the validity regimes of particular upscaled models.

In practice, it is quite common to consider a flow equation for the fracture surface with jump of the fluxes as the right hand side. This is a heuristic model that is obtained by the vertical averaging of the pressure equations inside the fracture so that the jump in the fluxes at the interfaces appear as a right hand side. However, this approach provides erroneous solutions

in the cases when α, β exceed certain values. To motivate this, we plot the error profile in Figure 1.1 for a 2D problem for different values of α, β. It is clearly shown in this plot that the error becomes large when $\alpha.\beta$ exceed 1.However, for $\alpha, \beta < 0$, the error remains low and this averaged model is an excellent approximation. This thesis performs computations backed by mathematical arguments to further provide insights into the ranges for α, β for which the different upscaled models approximate the reference solution with sufficiently high accuracy.

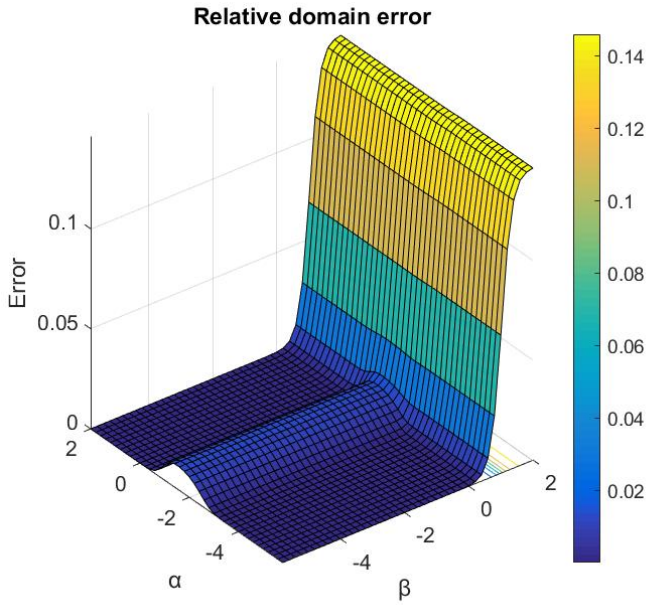

Figure 1.1: The relative domain error for different values of α and β for the average model. The error is computed with respect to the reference solution which is obtained by resolving explicitly the fracture geometry by taking finer mesh of the fracture geometry. The upscaled model is obtained by simple averaging along the vertical direction and assuming sufficiently small variation of the pressures in the vertical direction inside the fracture. This model is what is most often used in practice.

1.4 Outline

The thesis is structured as follows.

Chapter 2 - Introduction to fractured porous media

In this chapter we go through the basic concepts of rock and fluid properties and introduce the mathematical laws used to calculate flow through porous and fractured media. This chapter discusses the existing approaches for treating fractures.

Chapter 3 -Solution of a One-Dimensional case

Here we derive an analytical and a weak solution for the continuity equation in a simplified one-dimensional domain with a fracture of size 2ϵ and the permeability of $k = \epsilon^{\beta}$.

Chapter 4 -Solution of a Two-Dimensional case

The derivation in the previous chapter of the one-dimensional problem is extended to apply for a two-dimensional case. Weak solutions are defined in the two dimensional case and a rigorous upscaling is being performed by defining a dual problem. The dual problem is defined in a fixed domain with the coefficients depending upon ϵ. The derivation of the upscaled model depends on estimating the flux on the boundaries of this fixed domain. This approach is novel for deriving upscaled model for a fractured medium.

Chapter 5 -Numerical methods

This chapter discusses the numerical implementation of the upscaled models derived in the previous chapter for the 2D. Depending upon the exponent of the permeability scaling on the width of the fracture, there are different upscaled models that are derived. We discuss the numerical implementation for all the models that derived.

Chapter 6 -Simulations results

This chapter presents the numerical computations for different permeability ranges in the fracture corresponding to the results of the models described in Chapter 5. The computations are performed for the different scaling of permeabilities in the x- and y-direction. The reference solution is taken as the full model where the fractures are resolved by a finer discretization. The errors of the upscaled models are computed with respect to the references solution and are plotted. The impact of boundary conditions are discussed. We show how the boundary conditions and the different scaling for permeability interact with each other. We discuss the appropriate upscaled model that capture this behaviour.

Chapter 7 -Conclusion

The findings in this thesis is presented, and further extensions of this work is mentioned.

Chapter 2

Theory of Fractured Porous Media

2.1 Rock and Fluid Properties

2.1.1 Permeability

Permeability is a porous medium's capability to transmit fluids through its network of interconnected pores. This property is given as a tensor to describe the flow potential in different directions. The permeability can only be considered constant when there is only one fluid present. This is the absolute permeability. The permeability will change drastically if there are more than one component or one phase present, this is because of the interactions between the two components or phases. The flow potential of the two fluids is usually not the same. The fluid with the lowest flow potential may get trapped in the pores or even be able to block the path for the faster flowing fluid. A new concept is introduced, relative permeability. Relative permeability is the ratio between the effective permeability for one fluid in the rock and the absolute permeability for the rock (Zolotukhin & Ursin, 2000; Lien, 2004). In this thesis there will only be considered one fluid at a time, and the permeability is absolute permeability. The permeability matrix has to be a symmetric and positive definite according to Onsager's principle (Onsager, 1931). If the permeability is a scalar then the spatial direction does not play a role, and it is referred to as isotropic. Permeability is measured by Darcy and have the dimensions of a square length (m^2). Permeability is commonly denoted with $\mathbf{K}$ or k.

2.1.2 Porosity

Porosity is the measurement of the void space in a material. It is given as the fraction of the void volume with respect to the whole domain. The formula becomes

$$\phi = \frac{V_V}{V_T}, \tag{2.1}$$

where ϕ is the porosity, V_V is the void space and V_T is the total volume of the porous medium. The porosity is a ratio number between 0 and 1. The porosity is important in any industry working with porous media as it gives the potential for a rock or reservoir to store fluids like, oil, water or CO_2 (Zolotukhin & Ursin, 2000).

2.1.3 Representative Elementary Volume (REV) in Porous Media

A porous medium is not a homogeneous medium, and factors like the permeability and porosity can be hard to measure for the whole domain. These parameters are usually found using a sample from the reservoir. It is important that the sample is representative for the domain. If the sample where these parameters are measured is small, the results may get affected by microscopic effects. This can be due to a large void space, or a compact crystal that gives wrong

average values for the permeability and porosity. If the sample size is to large, it gets affected by macroscopic effects such as a huge fracture, or a layer of an other type of medium like for instance a different rock type. The sample size must be big enough to neglect microscopic effects, but still small enough to exclude macroscopic effects. A sample of this size is called a Representative Elementary Volume (REV) (Zolotukhin & Ursin, 2000). The REV is described in Figure 2.1

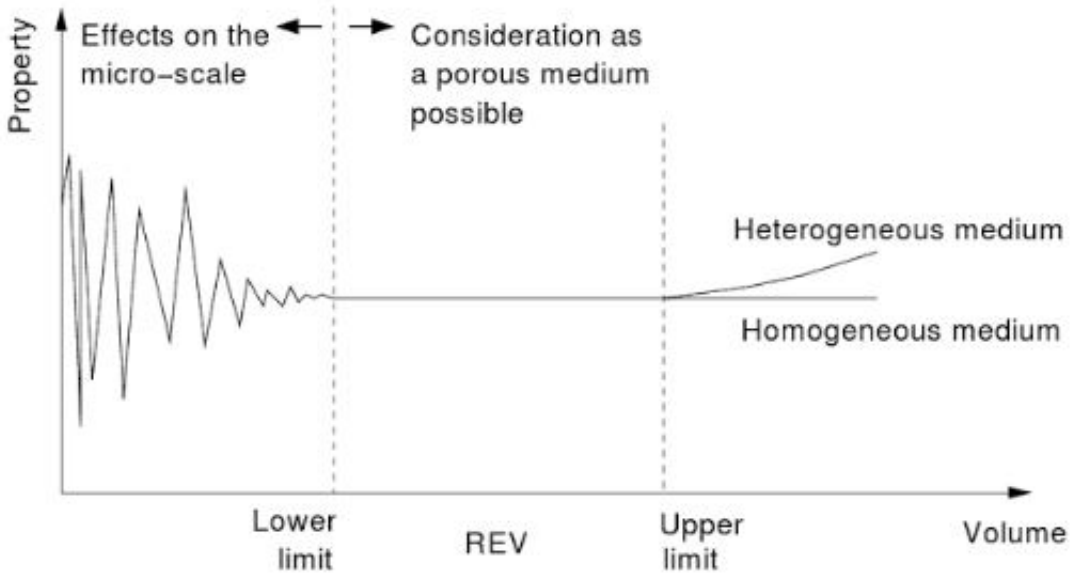

Figure 2.1: This figure shows how a representative elementary volume is picked (Dietrich et al., 2005)

2.1.4 Viscosity

Viscosity is defined as the fluids inner resistance to flow. Viscosity is usually given i centipoise (cp) where $1cp = 1mPa \times s$. Different types of fluids have different viscosity and different flow potential. Ketchup is said to be highly viscous while water is low viscous (Zolotukhin & Ursin, 2000).

2.2 Mathematical Laws for Flow in Porous Media

2.2.1 Darcy's Law

The formula for flux through a porous media was given by Henry Darcy in 1856. In his experiments he found that the flux through a rock was dependent on the the pressure difference on the sides of the rock, the permeability of the rock and the viscosity of the fluid that went through the rock (Nield & Bejan, 2006). Today the law is usually denoted as

$$\mathbf{u} = -\mathbf{K'}\nabla h \tag{2.2}$$

where $\mathbf{u}$ is the volumetric flux vector, $\mathbf{K'}$ is the hydraulic conductivity tensor and h the hydraulic head. The conductivity $\mathbf{K'}$ is dependent on the properties of the rock and fluid such as rock permeability $\mathbf{K}$, fluid viscosity μ and fluid density ρ. The hydraulic head is given as $h = \frac{p}{\rho g} + z$ where p is the pressure relative to some datum, g is the gravity constant and z is the elevation above the same datum (Nordbotten & Celia, 2012). For the cases in this thesis the gravitational constant is ignored, and the fluid is assumed to be incompressible. The Darcy's law is reduced to

$$\mathbf{u} = -\mathbf{K}\nabla p \tag{2.3}$$

It is important to include that Darcy's law is an empirical law which means that it is found by results from experiments. One of the most important assumptions of this law is that the flow has to flow relatively slow. The flow has to be laminar, and this occur if the Reynolds number is less than 1 (Nordbotten & Celia, 2012).

2.2.2 Conservation Equation

The conservation equation for mass is based on the concept that the change in mass within any given volume over any given time interval equals the flow of mass across the volume boundaries during that same time. In other words the function states that mass can not disappear or be created out of nothing. At a volume and time interval close to zero, the conservation equation becomes the continuity equation:

$$\frac{\partial(\rho\phi)}{\partial t} + \nabla \cdot (\mathbf{u}\rho) = q \tag{2.4}$$

where ρ is the density, ϕ is porosity, u is the volumetric fluid flow rate per unit of porous medium and q is some source term. The divergence operator $\nabla\cdot$ is applied to the mass flux vector $\mathbf{u}\rho$. The first term to the left of the equation is known as the accumulation term. This term will be zero in this thesis as we will deal with a steady state problem. If the fluids are assumed to be incompressible as well then equation 2.4 is reduced to

$$\nabla \cdot (\mathbf{u}) = q \tag{2.5}$$

By combining equation 2.3 and equation 2.5 this equation is obtained

$$\nabla \cdot (-\mathbf{K}\nabla p) = q \tag{2.6}$$

Thus the simulation of a simple isotherm single phase system only require the pressure variable (Kundu, Cohen, & Dowling, 2012).

2.2.3 Dimensionless Parameters

Knowledge of the relevant dimensionless parameters frequently aids the solution process, especially when assumptions and approximations are necessary to reach a solution. The dimensionless parameters obtained from the equation of fluid flow motion set the condition under which scale model testing with small models will prove useful for predicting the performance of larger devices. In particular, two flow fields are considered to be dynamically similar when their dimensionless parameters match, and their geometry are scale similar; that is, any length scale in the first flow field may be mapped to its counterpart in the second flow field by multiplication with a single scale ratio. When two flow fields are dynamically similar, analysis, simulations, or measurements from one flow field are directly applicable to the other when the scale ratio is accounted for. Moreover, use of standard dimensionless parameters typically reduces the parameters that must be varied in an experiment or calculation, and greatly facilitates the comparison of measured or computed results with prior work conducted under potentially different conditions (Kundu et al., 2012). Darcy's law can be made dimensionless by referring the

pressure to a maximal pressure on the upstream boundary, or the highest boundary pressure. There must be set a characteristic length, a reference permeability and a reference viscosity. Darcy's law becomes

$$\mathbf{u}^* = -\mathbf{K}^* \nabla^* p^* \tag{2.7}$$

where u^* is the dimensionless flux, K^* the dimensionless conductivity, p^* the dimensionless pressure and $\nabla^* = l\nabla$ where l is a reference length. The gravity is still neglected, and the viscosity is constant which means that the dimensionless viscosity becomes 1. The dimensionless conservation equation ends up becoming

$$q^* = \nabla^*(-\mathbf{K}^* \nabla^* p^*) \tag{2.8}$$

where q^* is a dimensionless source term (Tanaka, Ninokata, & Wada, 2002). In the rest of the thesis we will be working with dimensionless variables, and we will from now denote all dimensionless variables without the asteriks (*) symbol.

2.3 Fractures

The fractures in a porous media has a great impact on the mediums flow and transport abilities. Typically a fracture is a thin and long formation lying between two other formations. The fracture usually have different properties such as permeability and porosity from the rest of the domain. It is common to divide fractures into two different groups. Fractures with permeability higher than the surrounding and fractures with permeability lower than the surroundings. With a high permeability in the fracture, the flow tends to go into the fracture. In cases where the permeability is much higher, the flow can be assumed to only take place inside the fracture. When the permeability in the fracture is lower than the surroundings, flow will have the tendency not to enter the fracture and the fracture works as an aquitard or a sealing. The contact between the two sides of the fracture are not communicating, and that is why the pressure do not have to be continuous alongside the fracture interfaces. (Gudmundsson, Løtveit, & Gjesdal, 2002)

A fractured domain becomes a complexed domain to describe. The flow potential depends greatly on the properties of the fractures. Numerical simulations of mathematical models in these domains are challenging, takes a lot of time and needs a lot of computer capacity. The models get better and more precise for every specific data that is included. For problems where the fractures and the matrix are having almost equal properties, it can save some computer time to just homogenize the model. This approach however is not possible if the fractures and the matrix play significant roles for the flow. For these cases there will be better to calculate the flow through structures separately (Hægland, Assteerawatt, Dahle, Eigestad, & Helmig, 2009). For large open fractures, Darcy law may not be valid. The most common approach to solve for this types of fracture is to use the "cubic law". It is solved by applying the incompressible Navier-Stokes equations for a domain bounded by two parallel lines of length L, separated by a gap, d. For simplicity gravity is ignored, and we end up with

$$\rho(\frac{\partial \mathbf{u}}{\partial t} + \mathbf{u} \cdot \nabla p\mathbf{u}) = \nabla p + \mu \Delta \mathbf{u}. \tag{2.9}$$

By neglecting body forces, and assuring steady state conditions the equation becomes

$$\frac{\partial u_x}{\partial y} = \frac{p_2 - p_1}{\mu L} \tag{2.10}$$

This equation can be integrated twice to find the velocity profile across the fracture, and the velocity profile can be used to find the average velocity:

$$u_x(y) = \frac{1}{2\mu} \frac{p_2 - p_1}{L} [8\frac{d}{2}^2 - y], \tag{2.11}$$

$$\bar{u}_x = \frac{1}{2\mu}\frac{p_2 - p_1}{L}\frac{1}{d}\int_{-\frac{d}{2}}^{\frac{d}{2}}[(\frac{d}{2})^2 - y^2]dy = \frac{d^2}{12\mu}\frac{p_2 - p_1}{L}. \tag{2.12}$$

This is similar to the Darcy velocity because of the pressure gradient, and that a constant k^* can defined as $k^* = \frac{a^2}{12}$. k^* can be thought of as a modified permeability. The total flux is the average flux times the length of the gap which becomes

$$q_v = \frac{d^3}{12\mu}\frac{p_2 - p_1}{L}. \tag{2.13}$$

The cubic law was investigated further and for some cases there is necessary to include a frictional factor f, as well, like done by (Witherspoon, Wang, Iwai, & Gale, 1980). The cubic law is then denoted as

$$q_v = \frac{1}{f}\frac{d^3}{12\mu}\frac{p_2 - p_1}{L}. \tag{2.14}$$

2.3.1 Fracture Models

There are a lot of ways to include fractures in a model for porous media. This section will include a short description of some of the most common ways, including the discrete fracture model which will be applied in the simulations later in this thesis. Figure 2.3 shows how different types of porous media can be idealized. The idealized models are easier to describe with a mathematical approach.

2.3.2 The Equivalent Continuum Model

This model is based on the same concept as the REV model. The flux is modelled by a single continuum divided into small sub domains with uniform properties. These properties are found by averaging over all the subdomains. The subdomains must be significantly large so that the properties holds for the whole domain. This model has no explicit distinction between the fracture and the matrix, but they are both included in the averaging of the domain (Berkowitz, Bear, & Braester, 1988). An example of this method is described in (Samardzioska & Popov, 2005) where the porosity in the equivalent model is assumed to be

$$\phi_{equi} = \phi_m\frac{V_m}{V_t} + \phi_f\frac{V_f}{V_t} \tag{2.15}$$

where ϕ_m and ϕ_f denotes the porosity in the matrix and fracture respectively, V_m is the volume of the matrix, V_f the volume of the fracture and V_t the total volume of the REV domain. The hydraulic conductivity is given by

$$K_{equi} = K_m \cdot \frac{V_m}{V_t} + K_f \cdot \frac{V_f}{V_t} \tag{2.16}$$

where K_m and K_f are the hydraulic conductivities in the matrix and the fracture respectively. The results obtained using the equivalent continuum model represents the average values over the sufficiently large volumes of the domain, and it is therefore impossible to find the hydraulic head or concentration at a specific point.

2.3.3 The Dual Porosity Model

The dual porosity model is a model that consider the porosity in the rock and the fracture as two different porosity systems. The two porosity systems interact and exchange fluids with each other with respect to the hydraulic conductivity and the hydraulic head. The effective

hydraulic conductivity at the interface between fracture and the medium is described by Gerke and van Genuchten as

$$K_a = 0.5[K_{am} + K_{af}]. \tag{2.17}$$

where K_{am} and K_{af} are the hydraulic conductivities in the matrix and the fracture respectively with the distance a to the interface (Gerke & Genuchten, 1993). The flow between the two systems by using K_a in some type of darcy law. The flow occuring in the matrix is neglected when the flow potential of the domain is calculated because the flow potential is much higher in the fractures. The fractures have a great influence of the flow potential in the different directions in this model, and there is nessesary to include a directional permeability (Warren, Root, et al., 1963). This model is best exploited when there is a high porosity in the matrix and a low flow potential. The fractures however should have a high flow potential, but a low storage capacity (Warren et al., 1963).

2.3.4 The Multiple Interacting Continua Model

The Multiple Interacting Continua Model(MINC) is based on the dual porosity model and generalizes it by partitionate the grid cells into nests like shown in Figure 2.2. The grids are built up like this because the impact of the fracture is changing with the distance to the fracture. The impact of the fracture does not vary much in the direction parallel to the fracture, and that is why the grid cells are trying to be oriented parallel to the nearest fracture.(Pruess et al., 1985). This model is not strictly valid, but it can be a good approximation in many cases, it is designed to simulate fluid and heat flow. This type of grid is ideal to simulate flow processes such as imbibition and heat transfer, but it is not the best grid to capture flow with specific directionality such as gravity flow (Gong, Karimi-Fard, Durlofsky, et al., 2008).

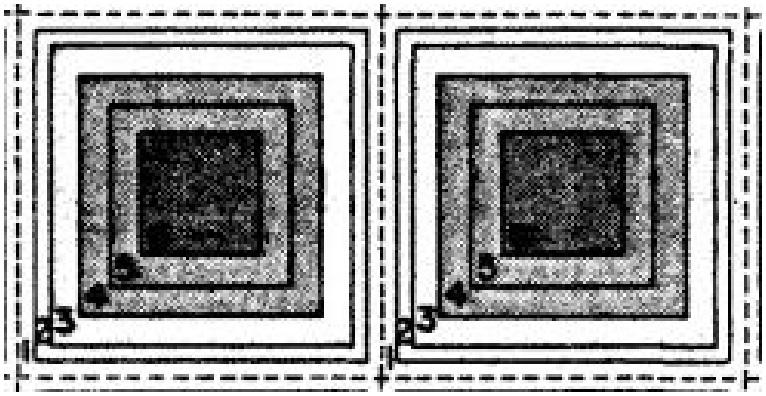

Figure 2.2: This figure shows how the grid cells in a MINC model is divided (Pruess et al., 1985).

2.3.5 Dual Porosity Dual Permeability Model

This model is equal to the dual porosity model, but it is a more general model which allows fluid flow in both the matrix and the fracture. In this way it requires more calculations, but it includes the cases where the flow potential in the matrix can not be neglected. The dual porosity, dual permeability consept has been used to model the flow of a single coponent in a single phase whitin a reservoir since around the 1960 (Hill, Thomas, et al., 1985; Barenblatt, Zheltov, & Kochina, 1960; Kazemi et al., 1969).

2.3.6 Discrete Fracture Model (DFM)

In this model, the fractured medium is assumed to be nonhomogeneous, and each fracture is calculated explicitly. For a complete reservoir there are usually a very large number of fractures, and there is impossible to calculate all the fractures separately. The complexity of the fracture makes it impractical to calculate every fracture separately and that is why this model is useful for systems where some fractures have a significant influence on the fluid flow. These fractures can be calculated explicit, while the rest of the fractures are neglected or calculated with using another approach. For the DFM the fluxes over the fracture interfaces are usually solved using a Darcy typed law like the one in section 2.3, or other versions of this law. The conservation equation is valid for the flow in the porous matrix and in the fracture (Samardzioska & Popov, 2005). Some discrete fracture models will be presented later.

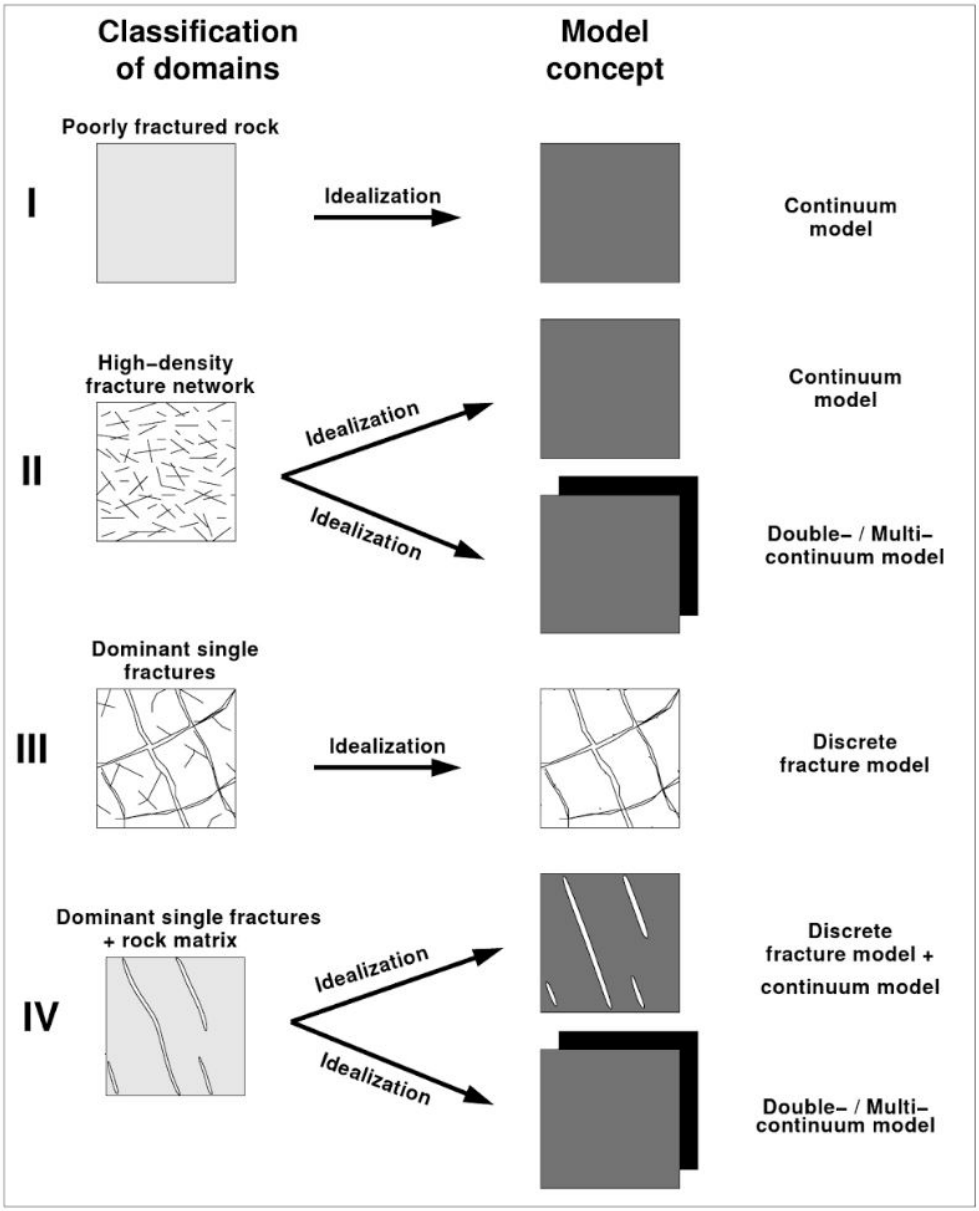

Figure 2.3: This figure shows how different classifications of domains can be separated into a ideal model. (Dietrich et al., 2005).

2.4 Context of this Thesis

The results of this thesis correspond to the framework of Discrete Fracture Model (DFM). The fractures therefore are explicitly modelled, however as lower dimensional surface embedded in a porous medium. Thus, in a 2D geometry of a rectangle, the fracture will be modelled as a 1D curve (line). In this 2D geometry, we have the Darcy flow model coupled to the flow equations on this fracture curve (line). The type of flow equation on the fracture depends on the fracture permeability. We derive a variety of upscaled fracture model based on the fracture permeability.

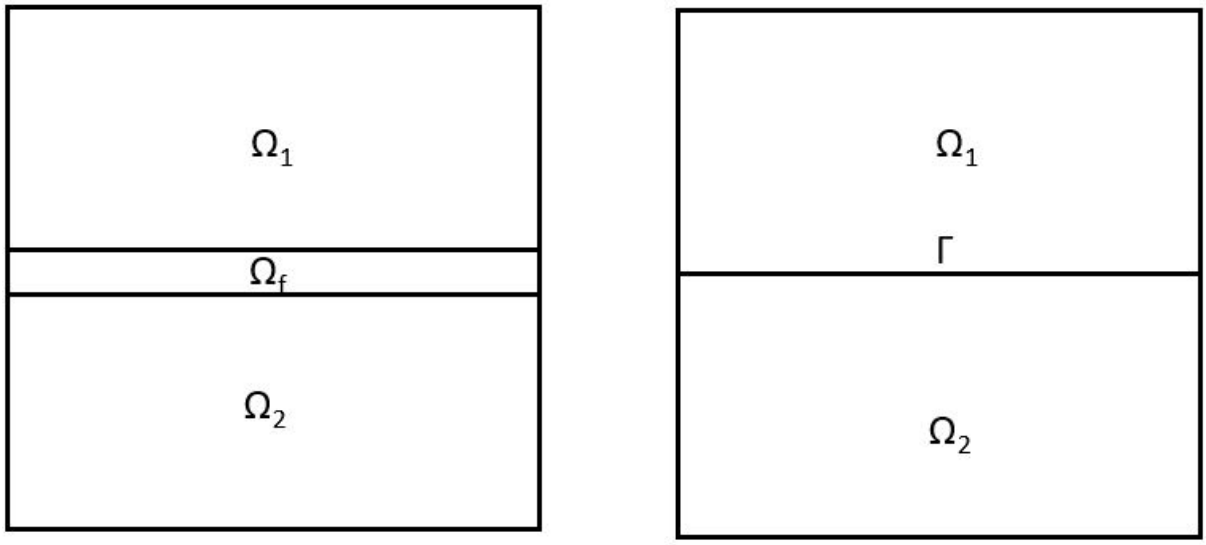

Figure 2.4: Fractured porous medium with the fracture treated as a part of the domain (left). On the right, the fracture is considered as a surface. In the fractured domain, the fracture permeability is taken as a tensorial permeability depending upon the width of the fracture. As the width decreases to zero, the limit mathematical model is represented pictorially on the right.

The permeability in the fracture is considered to be a diagonal tensor defined by:

$$K_f = \begin{bmatrix} \epsilon^{\alpha} & 0 \\ 0 & \epsilon^{\beta} \end{bmatrix}. \tag{2.18}$$

The fracture is considered as a thin domain Ω_f with small thickness ϵ shown in Figure2.4. Our approach is to consider upscaled models for different scalings given by α and β. These upscaled models are obtained by taking the limit ϵ tending to zero. The upscaled model is a mathematical limit obtained by this procedure of ϵ tending to zero.

To put our work in the context of existing literature, we cite the work of (Martin, Jaffré, & Roberts, 2005) dealing with the fractured flow. There is a formal derivation of the upscaled model. The reference model is given by

$$\begin{aligned} -\nabla \cdot (K_i \nabla p_i^{\epsilon}) &= q_i, \\ -\nabla \cdot (K_f \nabla p_f^{\epsilon}) &= q_f, \end{aligned}$$

coupled through the interface conditions between the fracture and porous matrix, $p_i = p_f$ and $-\nu_i \cdot K_i \nabla p_i - \nu_i \cdot K_f \nabla p_f = 0$ for $i = 1, 2$. Here ν_i is the normal at the fracture pointing from porous matrix Ω_i to the fracture domain Ω_f. The interface conditions are basically the continuity of pressure and the continuity of normal fluxes at the fracture-porous matrix interfaces. The

upscaled model for this model as derived formally in (Martin et al., 2005) consists of the following equations now defined in the domain $\Omega_1 \cup \Omega_2 \cup \Gamma_f$ where Γ_f is the fracture surface.

$$\begin{aligned} -\nabla \cdot (K_i \nabla p_i) &= q_i, \\ -\nabla \cdot (K_f \epsilon \nabla P_f) &= q_f + [K_i \nabla p_i], \\ (1-\xi)(-K_2 \nabla p_2) \cdot \nu_2 + \epsilon^{\beta-1}(p_i - p_f) &= \xi(-K_1 \nabla p_1) \cdot \nu_1, \text{ for } i = 1, 2. \end{aligned}$$

Here, $[K_i \nabla p_i] = -\nu_1 \cdot K_1 \nabla \cdot p_1 + \nu_2 \cdot K_1 \nabla \cdot p_1$ is the jump in the flux across the fracture surface Γ_f with ν_1 and ν_2 being the normals on the interface between Ω_i and fracture surface, respectively. For the present discussion, the most important thing to note here is that ξ is a fitting parameter between 0 and 1.

The derivation of the above upscaled model is based on two steps: the first step of integration along the normal to the fracture yields the jump in the flux term. The second step is a heuristic step where the pressure profile inside the fracture is *assumed* to satisfy a closure relationship given by the last equation. This closure relationship has ξ as the fitting parameter and may be used to fit the upscaled model as needed.

Our approach is different as we do not assume any profile of the fracture pressure. What we set out is by assuming a scale dependence of the permeability inside the fracture on the width ϵ and then use a *rigorous* approach for obtaining information regarding the profile of pressure inside the fracture and the limit behaviour as ϵ tends to zero. At the risk of repetition, we mention that considering the permeability tensor based on the width of the fracture should be interpreted as follows: let us say, we are given the permeability of the fracture. The question is what should be the average model that we should use for the fracture. The answer to this question depends on the scale of the permeability compared to the width of the fracture. We can therefore *determine the scale α and β* for the fracture permeability. Once, α and β are known, we can then determine the appropriate flow model to be used for the fracture surface. Contrary to the previous approach, our approach is rigorous and in fact even yields upscaled models that do not fit the closure condition that is assumed here.

Chapter 3

Analytical Solution and a Weak Formulation of the One-Dimensional Case

We begin with a one dimensional characterisation of the upscaled equations. A one dimensional case is not the most realistic model for a fracture in a porous medium. However it is an important case to study to see how different parameters influence the qualities of the reservoir, and how simplified methods can be applied to describe the fractures of different types. The one dimensional case that is studied in this chapter has a fracture of size 2ϵ and is described in figure 3.1. The permeability of the fracture is given by ϵ^β, in other words the size of the fracture to the power of β., and the permeability outside the fracture is for mathematical purposes equal to 1. In this chapter we will investigate the relation between the permeability and the size of the fracture as the size of the fracture goes to zero.

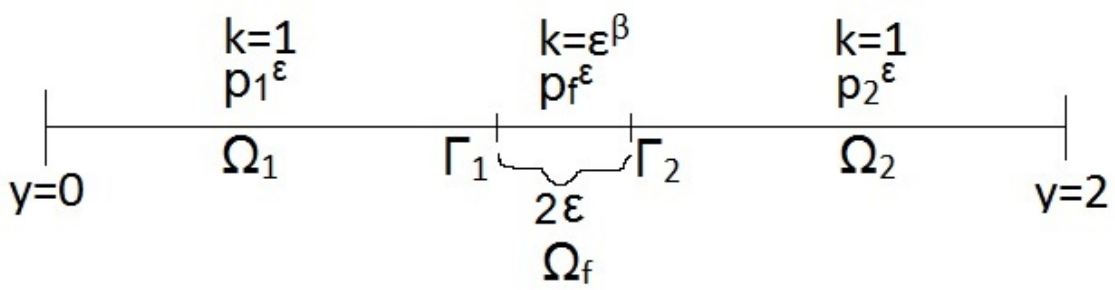

Figure 3.1: The domains Ω_1 and Ω_2 are separated by a domain Ω_f with permeability $k = \epsilon^\beta$

3.1 Derivation of the Analytical Case

In this section the one dimensional case for the fractured system will be solved analytically, and the solutions will be plotted for different values of β.

Problem Formulation

The problem in Figure 3.1 is described as

$$\begin{aligned} -\Delta p_1^\epsilon &= 0 \quad \text{where } y \in (0, 1-\epsilon) \\ -\Delta p_2^\epsilon &= 0 \quad \text{where } y \in (1+\epsilon, 2) \\ \epsilon^\beta \Delta p_f^\epsilon &= 0 \quad \text{where } y \in (1-\epsilon, 1+\epsilon) \end{aligned} \tag{3.1}$$

Interface and Boundary Conditions

The boundary conditions are

$$\begin{array}{ll} \text{at } y=0, & p_1^\epsilon = 1, \\ \text{at } y=2, & p_2^\epsilon = 0. \end{array} \tag{3.2}$$

The interface conditions on Γ_1, and Γ_2 are the continuity of fluxes and the continuity of pressures. The continuity of flux is given as,

$$\begin{array}{ll} \frac{\partial p_1^\epsilon}{\partial y} = \epsilon^\beta \frac{\partial p_f^\epsilon}{\partial y} & \text{at } \Gamma_1, \\ \frac{\partial p_2^\epsilon}{\partial y} = \epsilon^\beta \frac{\partial p_f^\epsilon}{\partial y} & \text{at } \Gamma_2. \end{array} \tag{3.3}$$

On the interfaces Γ_1 and Γ_2 the pressures are equal on the two sides, which means that $p_1^\epsilon = p_f^\epsilon$ on Γ_1 and $p_2^\epsilon = p_f^\epsilon$ on Γ_2.

$$\begin{array}{ll} p_1^\epsilon = p_f^\epsilon & \text{at } \Gamma_1, \\ p_2^\epsilon = p_f^\epsilon & \text{at } \Gamma_2. \end{array} \tag{3.4}$$

The differential equation for the pressures imply us that the pressure in all three sub domains Ω_1, Ω_2 and Ω_f are linear and can be written as,

$$p_i^\epsilon = c_i y + d_i, \tag{3.5}$$

where $i = 1, 2, f$.
The coefficients depend on ϵ, however we suppress this dependence for notational convenience.
The boundary condition for $p_1^\epsilon = 1$ at y=0 gives $d_1 = 1$. The boundary condition for p_2^ϵ implies $d_2 = -2c_2$. To find the other coefficients for the fracture we use the interface conditions:

$$\begin{array}{llll} \frac{\partial p_1^\epsilon}{\partial y} = \epsilon^\beta \frac{\partial p_f^\epsilon}{\partial y} & \text{at } \Gamma_1 & \text{yielding} & \epsilon^\beta c_f = c_1, \\ \frac{\partial p_2^\epsilon}{\partial y} = \epsilon^\beta \frac{\partial p_f^\epsilon}{\partial y} & \text{at } \Gamma_2 & \text{giving} & \epsilon^\beta c_f = c_2. \end{array} \tag{3.6}$$

Recall that the permeability in Ω_1 and Ω_2 is given as one. Using this gives $\epsilon^\beta c_f = c_1 = c_2$. The constants c_f and d_f can be determined employing the continuity of pressure at Γ_1 and Γ_2. The interfaces Γ_1 and Γ_2 exists at $y = 1-\epsilon$ and $y = 1+\epsilon$ respectively, which gives

$$\begin{array}{ll} c_1 y + d_1 = c_f y + d_f & \text{at } y = 1-\epsilon, \\ c_2 y + d_2 = c_f y + d_f & \text{at } y = 1+\epsilon. \end{array} \tag{3.7}$$

On the interfaces at $y = 1 \pm \epsilon$, and from equation (3.6), we have that $c_1 = \epsilon^\beta c_f = c_2$ and that $d_1 = 1$. For $(3.7)_1$ this gives that

$$\begin{array}{rl} c_1(1-\epsilon) + 1 & = c_1 \epsilon^{-\beta}(1-\epsilon) + d_f, \\ d_f & = c_1(1-\epsilon) + 1 - c_1\epsilon^{-\beta}(1-\epsilon), \\ d_f & = c_1(1-\epsilon)(1-\epsilon^{-\beta}) + 1, \end{array} \tag{3.8}$$

and from $(3.7)_2$

$$\begin{array}{rl} c_2(1+\epsilon) - 2c_2 & = c_2\epsilon^{-\beta}(1+\epsilon) + d_f, \\ d_f & = c_2(1+\epsilon)(1-\epsilon^{-\beta}) - 2c_2. \end{array} \tag{3.9}$$

The information in (3.8) and (3.9) can be used to solve for the constants c_1 and c_2:

$$c_1(1-\epsilon)(1-\epsilon^{-\beta}) + 1 = c_2(1+\epsilon)(1-\epsilon^{-\beta}) - 2c_2$$

which gives that

$$c_1 = c_2 = \frac{-1}{2(\epsilon^{-\beta+1} - \epsilon + 1)}, \tag{3.10}$$

and that

$$c_f = \frac{-\epsilon^{-\beta}}{2(\epsilon^{-\beta+1}-\epsilon+1)}, \tag{3.11}$$

The relation in (3.10), can be inserted into (3.8) and (3.9) to give the value of the last unknown constant, d_f.

3.1.1 Different Cases for Different β Values

The calculations above involve different exponents of ϵ in the coefficients. This suggests five different cases for different β values which need to be studied further to get an understanding of how the flux behaves as $\epsilon \to 0$ in all cases. We list all these cases,

$$\begin{array}{ll} \text{case 1:} & \beta = 0 \\ \text{case 2:} & \beta < 0 \\ \text{case 3:} & 0 < \beta < 1 \\ \text{case 4:} & \beta = 1 \\ \text{case 5:} & \beta > 1 \end{array}$$

that will be considered below.

Case 1, $\beta = 0$

In the first case, the formulation for the slope c_1 in (3.10) gives that

$$c_1 = \frac{-1}{2(\epsilon^1 - \epsilon + 1)},$$

which means that in the limit of ϵ tending to zero, c_1 tends to $-\frac{1}{2}$. The slope in the fracture, c_f, can be calculated using (3.11) which gives that

$$c_f = \epsilon^0 \frac{-1}{2(\epsilon^1 - \epsilon + 1)}.$$

The slope c_f, thus, approaches $-\frac{1}{2}$. Hence, in this case the slope is the same in all three domains, and equation (3.8) gives that

$$d_f = \frac{1}{2}(1-\epsilon)(1-\epsilon^{-0}) + 1 \Rightarrow d_f = 1.$$

The pressure is continuous and a plot of the pressure is shown in Figure 3.2.

Case 2, $\beta < 0$

In this case (3.10) and (3.11) gives that $c_1 \to -\frac{1}{2}$, $c_f \to 0$ and

$$d_f = -\frac{1}{2}(1-0)(1-0) + 1 = \frac{1}{2}$$

Then

$$\lim_{\epsilon \to 0} p_f^\epsilon = \frac{1}{2}$$

The pressure is constant in Ω_f and have a slope of $-\frac{1}{2}$ in Ω_1 and Ω_2. The pressure becomes continuous as $\epsilon \to 0$. This case is also shown in Figure 3.2

Case 3, $0 < \beta < 1$

In this case (3.11) gives that c_1 goes to $-\frac{1}{2}$ as $\epsilon \to 0$ but $\epsilon^{-\beta}$ blows up. This means that

$$c_f \to -\infty, d_f = c_1(1-\epsilon)(1-\epsilon^{-\beta}) + 1 \to \infty,$$

that is, both c_f and d_f blow up but in different directions. We need to estimate p_f^ϵ at $y = 1$ using (3.5). Both the coefficients c_f and d_f blow up, nevertheless, p_f^ϵ may have a finite limit. We readily check this by a straightforward computation.

$$\lim_{\epsilon \to 0} p_f^\epsilon = c_f + d_f. \tag{3.12}$$

By inserting values for c_f and d_f we get that

$$\begin{aligned} p_f^\epsilon = & \frac{-\epsilon^{-\beta}}{2(1-\epsilon+\epsilon^{-\beta})} + c_1(1-\epsilon)(1-\epsilon^{-\beta}) + 1, \\ = & 1 + \frac{-\epsilon^{-\beta} - (1-\epsilon+\epsilon^{-\beta+1}-\epsilon^{-\beta})}{2(1-\epsilon^{-\beta+1}-\epsilon)}, \\ \to & \frac{1}{2}. \end{aligned} \tag{3.13}$$

The pressure profile is linear for this case as well. The pressure in Ω_f converge to $\frac{1}{2}$ as the size of Ω_f shrinks to zero. The pressure is shown in Figure 3.2.

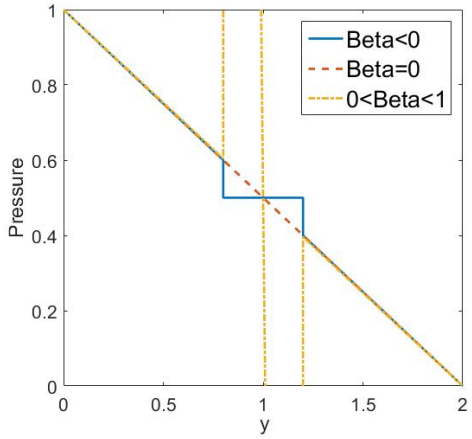

(a) Shows the behaviour of the pressure for cases 1, 2, and 3 inside the three domains

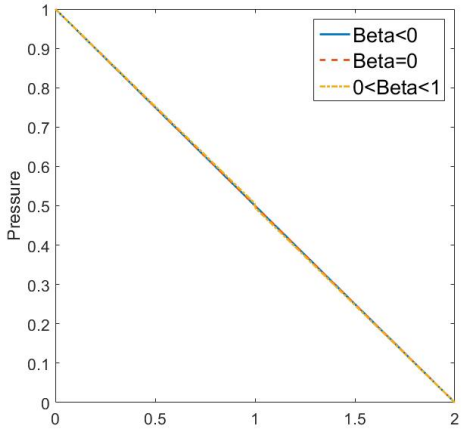

(b) Shows the pressure profile in the whole domain.

Figure 3.2: The first three cases are all converging to the same linear solution with $c = -\frac{1}{2}$ as the slope of the line. In all the three cases, essentially, the fracture is not playing any role and in the limit behaves as if it is absent.

As expected, in all the three cases, for fixed β, the pressure profiles are different. In the case when the permeability is blowing up (for the case when $\beta < 0$), the pressure profile inside the fracture is flat connected to linear profiles to the end points of the whole domain in the two sides of the fracture domain, respectively. Note that in the three cases, the permeability inside the fracture is either 1 (for the case when $\beta = 0$) or blowing up ($\beta < 0$), or vanishes $\beta > 0$. Interesting enough, all the cases for which $\beta < 1$ converge to the same solution as $\epsilon \to 0$, that is, a linear profile. This shows that the case when $\beta < 1$ provides sufficient permeability for the pressure to equilibrate and retain the continuity of the pressure inside the fracture. As the size of this fracture shrinks, the pressures at the ends of the fractures become closer and in the limit simply yield the same solution as if they are absent.

Case 4, $\beta = 1$

Using (3.11) we get

$$c_1 = c_2 = \frac{-1}{2(1-\epsilon+\epsilon^0)} = -\frac{1}{4}.$$

The expressions for p_1^ϵ and p_2^ϵ given by (3.5) becomes

$$p_1^\epsilon(y) = c_1 + d_1 = 1 - \frac{1}{4}y \tag{3.14}$$

and

$$p_2^\epsilon(y) = c_2 y + d_2 = -\frac{1}{4}y + (-2c_2) = \frac{1}{2} - \frac{1}{4}y. \tag{3.15}$$

The slope c_f of the pressure in Ω_f^ϵ becomes $-\infty$ as ϵ vanishes. At $y = 1$, (3.14) and (3.15) provide

$$\lim_{\epsilon\to 0} p_1^\epsilon(y=1) = \tfrac{3}{4} \quad \lim_{\epsilon\to 0} p_2^\epsilon(y=1) = \tfrac{1}{4}. \tag{3.16}$$

Unlike in the previous three cases, in this case the two subdomain pressures at the interface are discontinuous. However, the role of the fracture is not yet explored. In fact, what turns out is that the fracture pressure will provide the coupling condition for the two discontinuous pressures at the interface from the subdomain sides. We have from (3.8) that d_f

$$d_f = c_1(1-\epsilon)(1-\epsilon^{-\beta}) + 1. \tag{3.17}$$

By inserting for c_1, set $\beta = 1$, (3.17) can be reduced to

$$d_f = \frac{1}{2} + \frac{1}{4\epsilon}. \tag{3.18}$$

The formula for p_f^ϵ becomes

$$p_f^\epsilon = \frac{1}{4\epsilon}(1-y) + \frac{1}{2}. \tag{3.19}$$

Since both $(1-y)$ and ϵ go to zero as the size of fracture shrinks, we define a re-scaled variable

$$\gamma = \frac{1-y}{\epsilon}. \tag{3.20}$$

The usefulness of this definition becomes immediately clear by noticing that

$$\begin{array}{lll} 1-y=0 & \to & \gamma = 0, \\ 1-y=\epsilon & \to & \gamma = -1, \\ 1+y=\epsilon & \to & \gamma = 1. \end{array} \tag{3.21}$$

This, the variable γ maps the fracture geometry to a fixed domain size of $[-1, 1]$. In terms of this new variable γ, the expression for p_f^ϵ can be written as

$$p_f^\epsilon(\gamma) = -\frac{\gamma}{4} + \frac{1}{2}. \tag{3.22}$$

Note that the pressures at the end points (interfaces) become

$$p_f^\epsilon(\gamma) = \tfrac{3}{4} \quad \text{on} \quad \gamma = -1 \tag{3.23}$$

and

$$p_f^\epsilon(\gamma) = \tfrac{1}{4} \quad \text{on} \quad \gamma = +1. \tag{3.24}$$

The continuity of the pressures at the interface is preserved since

$$\begin{array}{c} p_1(y=1) = p_f(\gamma=-1) \\ p_2(y=1) = p_f(\gamma=1). \end{array} \tag{3.25}$$

The pressure profile is plotted in Figure 3.3. This case is perhaps more interesting than the first three cases described above. As we have seen in this case, the fracture is playing an important role. Seen from the limit domain perspective, there is a discontinuity of pressure at the interface at the point to which fracture domain has shrunk to. However, in this case, the fracture can not be ignored in the limit, unlike in the previous three cases. In fact the upscaled model has a "two-scale" behaviour where the fracture pressure profile connects the discontinuities. From the point of view of whole domain, there is simply a discontinuity in the pressure profile, but *at the point of discontinuity*, there is another scale that once *zoomed-in* provides a fracture pressure profile justifying the "two-scale" behaviour.

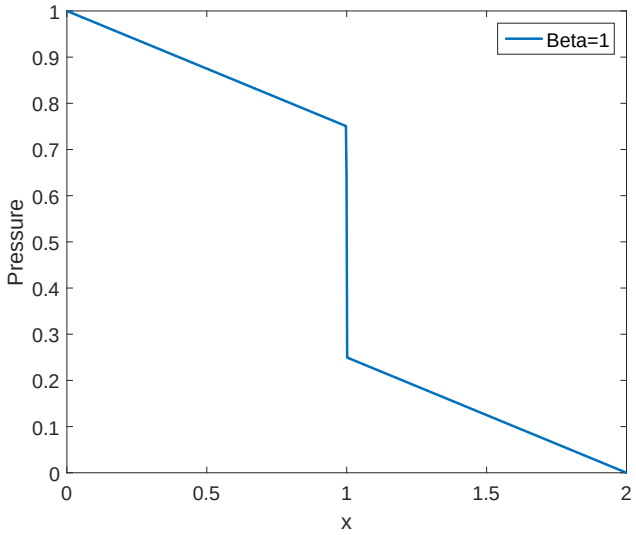

Figure 3.3: Pressure profile in the whole domain for the case $\beta = 1$. Note that there is a discontinuity of pressure at the fracture interface. In this case, the fracture can not be ignored in the limit, unlike in the previous three cases. In fact the upscaled model has a "two-scale" behaviour where the fracture pressure profile connects the discontinuities. From the point of view of whole domain, there is simply a discontinuity in the pressure profile, but *at the point of discontinuity*, there is another scale that once *zoomed-in* provides a fracture pressure profile justifying the "two-scale" behaviour.

This shows that the model for the fracture pressure in the case $\beta = 1$ can be written as

$$\frac{d^2 p_f^\epsilon}{d\gamma^2} = 0 \tag{3.26}$$

with the interface conditions, the continuity of pressure

$$p_f = p_1(y = 1) \text{ at } \gamma = -1 \text{ and } p_f = p_2(y = 1) \text{ at } \gamma = 1$$

together with the flux continuity

$$\frac{dp_f}{d\gamma} = \frac{dp_1}{dy}(y = 1) \text{ at } \gamma = -1 \text{ and } \frac{dp_f}{d\gamma} = \frac{dp_2}{dy}(y = 1) \text{ at } \gamma = 1.$$

Needless to say, we can solve the above equation analytically giving us a linear profile. However, we prefer to put this in the form above to enable its comparison and extension in the 2D case. This case will be investigated further in the two scaled model in Section 5.1.2.

Case 5, $\beta > 1$

From (3.10), the slopes in Ω_1 and Ω_2 given by

$$c_1 = c_2$$

go to zero because $\epsilon^{-\beta} = \infty$ as $\epsilon \to 0$. we conclude using(3.5) that the pressures are constant in Ω_1 and Ω_2. Hence the two models become decoupled. At this stage, the fracture pressure becomes irrelevant as far as the upscaled models are concerned.
Nevertheless, we proceed to identify what happens in the fracture. The value of c_f^ϵ becomes:

$$c_f^\epsilon = \epsilon^{-\beta} c_1$$

and for d_f we get that:

$$d_f = c_1(1-\epsilon)(1-\epsilon^{-\beta}) + 1.$$

For p_f^ϵ at $y = 1$ this gives

$$\begin{aligned} p_f^\epsilon = & \frac{-\epsilon^{-\beta}}{2(1-\epsilon+\epsilon^{-\beta})} + c_1(1-\epsilon)(1-\epsilon^{-\beta}) + 1 \\ = & 1 + \frac{-\epsilon^{-\beta} - (1-\epsilon+\epsilon^{-\beta+1}-\epsilon^{-\beta})}{2(1+\epsilon^{-\beta+1}-\epsilon)} \\ = & \frac{1}{2}. \end{aligned} \tag{3.27}$$

At the interfaces $y = 1-\epsilon$ and $y = 1+\epsilon$, we have that $p_f^\epsilon = 1$ and $p_f^\epsilon = 0$ respectively, and the solution becomes

$$\begin{aligned} p_1^\epsilon = d_1^\epsilon = 1 \quad & \text{in } \Omega_1, \\ p_2^\epsilon = d_2^\epsilon = 0 \quad & \text{in } \Omega_2, \\ p_f^\epsilon = \frac{1}{\epsilon} y + 1 \quad & \text{in } \Omega_f. \end{aligned} \tag{3.28}$$

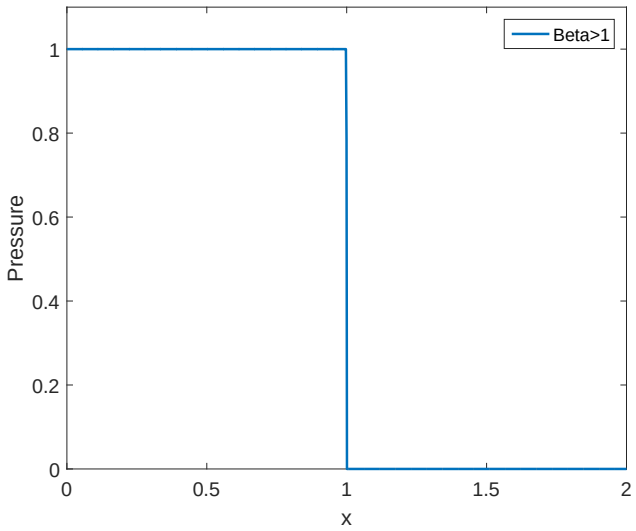

Figure 3.4: Pressure in 1D with $\beta > 1$.

The figure shows that this case gives a constant pressure in Ω_1^ϵ and Ω_2^ϵ. As stated before, the two domains are decoupled and can be solved independently. Thus, in this case, the fracture acts as a "barrier". It is interesting to note that the fracture pressure is simply the average of the two pressures at the interfaces from the subdomain sides.

3.2 An Alternative Approach: using Dual Problem

Next, we describe a novel approach to obtain the upscaled model in a fractured porous medium. This approach is based on (Chen et al., 2012) has certain advantages. In this reference, the authors have used similar approach for finding the insulating effect of a thin coating around a thermally conducting two dimensional body. The difference between the results in this reference and our approach is that in our case, the fracture is a part of the domain and is sandwiched between two subdomains. This is in contrast to the case considered in this reference where the thin insulating layer in the limit shrinks to be a boundary and the limit problems provide the boundary conditions. In the case of fractures, we obtain an interface condition that couples the two subdomains. Even though the derivation here is presented for a 1D case it can be extended to 2D case with suitable alterations, at least in certain cases. Secondly and perhaps more importantly, this approach provides a rather general framework for other type of equations.

This alternative approach consists of three steps: 1. We define a weak formulation for the model problem, 2. We define a dual boundary value problem in the fracture domain based on the model equations, and finally 3. We estimate the fluxes at the boundaries of the fracture domain. Note that the dual problem is defined only in the fracture domain with suitable boundary conditions allowing us to decouple the fracture domain from the other subdomains. This study of isolated fracture domain provides a partial differential equation with suitable boundary values. Thus, the study of upscaled model is reduced to studying the dual boundary value problem and estimating the fluxes at the boundaries.

We begin by defining a weak formulation for 1D problem. This alternative approach of a 1D case uses a lot of the same principles as in the 2D case. We therefore provide the full details of such an approach for the 1D weak case in this thesis, and later extend it to a two dimensional case. Our primary reference for the approach of defining this dual problem is (Chen et al., 2012).

Problem Formulation

$$\begin{aligned} \frac{\partial^2 p_1^\epsilon}{\partial y^2} &= 0 \quad \text{where } y \in (0, 1-\epsilon) \\ \frac{\partial^2 p_2^\epsilon}{\partial y^2} &= 0 \quad \text{where } y \in (1+\epsilon, 2) \\ \epsilon^\beta \frac{\partial^2 p_f^\epsilon}{\partial y^2} &= 0 \quad \text{where } y \in (1-\epsilon, 1+\epsilon) \end{aligned} \tag{3.29}$$

Boundary and Interface Conditions

$$\begin{aligned} p_1^\epsilon &= 1 \quad \text{at } y = 0 \\ p_2^\epsilon &= 0 \quad \text{at } y = 2 \\ p_1^\epsilon &= p_f^\epsilon \quad \text{at } y = 1-\epsilon \\ p_2^\epsilon &= p_f^\epsilon \quad \text{at } y = 1+\epsilon \\ \frac{\partial p_1^\epsilon}{\partial y} &= \epsilon^\beta \frac{\partial p_f^\epsilon}{\partial y} \quad \text{at } y = 1-\epsilon \\ \frac{\partial p_2^\epsilon}{\partial y} &= \epsilon^\beta \frac{\partial p_f^\epsilon}{\partial y} \quad \text{at } y = 1+\epsilon \end{aligned} \tag{3.30}$$

3.2.1 Weak Formulation

The definition of a weak formulation is quite standard. First we consider the pressure p_1^ϵ that is inside the domain Ω_1, and introduce a test function ψ_1 and multiply both sides of the pressure equation (3.29). The test function ψ_1 is chosen to be infinitely smooth, that is, $\psi_1 \in C^\infty(\Omega_1)$. Later we will put restrictions on the boundary condition on ψ_1 (that is, $\psi_1 = 0$ at $y = 0$) in sync with the Dirichlet boundary condition for p_1^ϵ at that point. Applying integration by parts

gives, for all smooth test functions ψ_1,

$$\int_0^{1-\epsilon} \frac{\partial p_1^\epsilon}{\partial y}\frac{\partial \psi_1}{\partial y} + \frac{\partial p_1^\epsilon}{\partial y}\psi_1(y=1-\epsilon) - \frac{\partial p_1^\epsilon}{\partial y}\psi_1(y=0) = 0. \tag{3.31}$$

Now choosing the test function, $\psi_1(y=0)=0$ allows us to get rid of the boundary term at $y=0$ and (3.31) becomes

$$\int_0^{1-\epsilon} \frac{\partial p_1^\epsilon}{\partial y}\frac{\partial \psi_1}{\partial y} + \frac{\partial p_1^\epsilon}{\partial y}\psi_1(y=1-\epsilon) = 0 \tag{3.32}$$

for all smooth test functions ψ_1. Similar steps for the equation defined in $\Omega_2^\epsilon = (1+\epsilon, 2)$, followed by choosing $\psi_2(y=2)=0$ we get

$$\int_{1+\epsilon}^{2} \frac{\partial p_2^\epsilon}{\partial y}\frac{\partial \psi_2}{\partial y} - \frac{\partial p_2^\epsilon}{\partial y}\psi_2(y=1+\epsilon) = 0, \tag{3.33}$$

for all smooth test functions ψ_2. For $\Omega_f^\epsilon = (1-\epsilon, 1+\epsilon)$ the equation becomes

$$\int_{1-\epsilon}^{1+\epsilon} \epsilon^\beta \frac{\partial p_f^\epsilon}{\partial y}\frac{\partial \psi_f}{\partial y} + \epsilon^\beta \frac{\partial p_f^\epsilon}{\partial y}\psi_f(y=1-\epsilon) - \epsilon^\beta \frac{\partial p_1^\epsilon}{\partial y}\psi_f(y=0) = 0 \tag{3.34}$$

for all smooth test functions ψ_f. Let us denote the term containing integrals in (3.32), (3.33) and (3.34) (first term in each of these equations) by I_1^ϵ, I_2^ϵ, and I_f^ϵ, respectively. Let the test functions satisfy the continuity conditions, $\psi_1 = \psi_f$ at $y = 1-\epsilon$ and $\psi_2 = \psi_f$ at $y = 1+\epsilon$. Using flux continuity at the interfaces, by summing the three equations, we obtain

$$I_1^\epsilon \quad + \quad I_2^\epsilon \quad + \quad I_f^\epsilon \quad = 0 \tag{3.35}$$

The above variational form provides us with the following bounds by testing with $\psi_1 = p_1^\epsilon, \psi_2 = p_2^\epsilon, \psi_f = p_f^\epsilon$.

lemma 1. *There exists a $C > 0$ such that $p_1^\epsilon, p_2^\epsilon, p_f^\epsilon$ satisfy the following estimates,*

$$\|\nabla p_1^\epsilon\|^2 + \|\nabla p_2^\epsilon\|^2 + \|\epsilon^\beta \nabla p_f^\epsilon\|^2 \leq C.$$

The above boundedness result readily provides us with the following convergence result.

lemma 2. *There exists p_1, p_2 such that, up to a subsequence, as ϵ goes to zero, $p_1^\epsilon, p_2^\epsilon$ converge to p_1, p_2 weakly in H^1 and thus, strongly in L^2 in their respective domains of definition.*

As stated before, we will now define a dual problem. This problem is defined by considering I_f^ϵ, and using integration by part we get,

$$I_f^\epsilon \quad = \int_{1-\epsilon}^{1+\epsilon} p_f^\epsilon \tfrac{d}{dy}(\epsilon^\beta \tfrac{d\psi_f}{dy}) + p_f^\epsilon \epsilon^\beta \tfrac{d\psi_f}{dy}(1+\epsilon) - p_f^\epsilon \epsilon^\beta \tfrac{d\psi_f}{dy}(1-\epsilon). \tag{3.36}$$

The basic idea is now to let ψ_f satisfy an equation so that the integral term vanishes. This easily motivates the following definition of the dual problem.

3.2.2 Dual problem

Definition 1. The dual problem consists of finding ξ satisfying $\frac{d}{dy}(\epsilon^\beta \frac{d\xi}{dy}) = 0$ in Ω_f^ϵ, along with the boundary conditions $\xi = \psi_1$ at $y = 1-\epsilon$ and $\xi = \psi_2$ at $y = 1+\epsilon$.

It is clear that for any smooth ψ_1, ψ_2, there exists a unique and smooth ξ satisfying the above equation. A natural question is if the set of such ξ's form a dense subset of smooth test functions. This is easily confirmed once we notice that for any smooth ψ_f, there exists a unique decomposition $\psi_f = \xi + \eta$ with η solving a poisson equation with ψ_f as the right hand side with zero Dirichlet boundary conditions. Thus, for any ψ_f there is a unique correspondence with ξ with ξ being also smooth.

For ψ_f solving the dual problem defined above, I_f^ϵ reduces to

$$I_f = p_f^\epsilon \epsilon^\beta \frac{d\psi_f}{dy}(1+\epsilon) - p_f^\epsilon \epsilon^\beta \frac{d\psi_f}{dy}(1-\epsilon) \tag{3.37}$$

Note that the above terms are nothing but the fluxes at the fracture/subdomain interfaces. The dual problem can be solved to give ψ_f satisfying

$$\begin{aligned} &\tfrac{d}{dy}(\epsilon^\beta \tfrac{d\psi_f}{dy}) = 0, \\ &\Rightarrow \epsilon^\beta \tfrac{d\psi_f}{dy} = c_f \\ &\Rightarrow \psi_f = \tfrac{c_f}{\epsilon^\beta} y + d_f \end{aligned} \tag{3.38}$$

for some constants c_f, d_f. They will be determined by the boundary conditions. At the left intersections Γ_1 we have the following boundary condition

$$\psi_f(y = 1-\epsilon) = \frac{c_f}{\epsilon^\beta}(1-\epsilon) + d_f$$

and at Γ_2

$$\psi_f(y = 1+\epsilon) = \frac{c_f}{\epsilon^\beta}(1 + \epsilon_+ d_f.$$

Let us denote

$$g_1 := \psi_f(y = 1-\epsilon),\ g_2 := \psi_f(y = 1+\epsilon).$$

The above two conditions lead to two linear equations involving two unknowns c_f, d_f. Solving for them, we get

$$c_f = -\frac{\epsilon^{\beta-1}}{2}(g_1 - g_2), \tag{3.39}$$

$$d_f = \frac{1}{2}(g_1 + g_2) + \frac{1}{2\epsilon}(g_1 - g_2). \tag{3.40}$$

The function, ψ_f, can be found by inserting (3.39) and (3.40) into (3.38), and is given by

$$\psi_f = \frac{c_f}{\epsilon^\beta} y + d_f = \frac{g_1 - g_2}{2\epsilon}(1-y) + \frac{1}{2}(g_1 + g_2). \tag{3.41}$$

From (3.38) and (3.39) it is given that c_f satisfies,

$$\epsilon^\beta \frac{d\psi_f}{dy} = c_f = -\frac{\epsilon^{\beta-1}}{2}(g_1 - g_2). \tag{3.42}$$

By replacing $\epsilon^\beta \frac{d\psi_f}{dy}$ with $-\frac{\epsilon^{\beta-1}}{2}(g_1 - g_2)$ in (3.37), I_f^ϵ is given by

$$I_f^\epsilon = -\frac{1}{2}\epsilon^{\beta-1}(g_1 - g_2)[p_2^\epsilon(y = 1+\epsilon) - p_1^\epsilon(y = 1-\epsilon)], \tag{3.43}$$

which can be inserted into (3.35) to obtain the following relation

$$I_1^\epsilon + I_2^\epsilon = \frac{1}{2}\epsilon^{\beta-1}(g_1 - g_2)[p_2^\epsilon(y = 1+\epsilon) - p_1^\epsilon(y = 1-\epsilon)] \tag{3.44}$$

This problem can be separated into three different cases, based on the exponent involved in the above expression, $\beta > 1$, $\beta < 1$ and $\beta = 1$. For the discussions below, recall the existence of limits p_1, p_2, p_f obtained as the limit of $p_1^\epsilon, p_2^\epsilon, p_f^\epsilon$ as ϵ vanishes.

Case 1, $\beta > 1$

The first case when $\beta > 1$ gives from (3.44) that $I_1^\epsilon + I_2^\epsilon \to 0$ as $\epsilon \to 0$ (since I_f^ϵ vanishes as ϵ tends to zero). This gives that

$$\lim_{\epsilon\to 0} \int \frac{dp_1^\epsilon}{dy}\frac{d\psi_1}{dy} + \lim_{\epsilon\to 0} \int \frac{dp_2^\epsilon}{dy}\frac{d\psi}{dy} = 0, \tag{3.45}$$

which gives us

$$\lim_{\epsilon\to 0}(-\frac{d^2p_1^\epsilon}{dy^2}, \psi_1)_{\Omega_1^\epsilon} + \lim_{\epsilon\to 0}\frac{dp_1^\epsilon}{dy}\psi_1(y=1) - \lim_{\epsilon\to 0}(\frac{d^2p_2^\epsilon}{dy^2}, \psi_2)_{\Omega_2^\epsilon} - \lim_{\epsilon\to 0}\frac{dp_2^\epsilon}{dy}\psi_2(y=1) = 0. \tag{3.46}$$

The test function ψ_1 is chosen such that $\psi_1 = 0$ on $\partial\Omega_1$ and further choose $\psi_2 \equiv 0$. This implies in the limit case when Ω_1^ϵ becomes Ω_1,

$$\int_{\Omega_1} -\frac{d^2p_1}{dy^2}\psi_1 = 0, \tag{3.47}$$

or in strong form in the limit case,

$$-\frac{d^2p_1}{dy^2} = 0 \text{ in } \Omega_2 \tag{3.48}$$

retrieving the original equation in the limit case in the subdomain.

Next, as in the previous case, the test function ψ_2 is chosen such that $\psi_2 = 0$ on $\partial\Omega_2$ and $\psi_1 \equiv 0$ leading to, for all smooth test functions ψ_2

$$\int_{\Omega_2} -\frac{d^2p_2}{dy^2}\psi_2 = 0, \tag{3.49}$$

or in strong form in the limit case,

$$-\frac{d^2p_2}{dy^2} = 0 \text{ in } \Omega_2. \tag{3.50}$$

The only thing left in (3.46) is

$$(\frac{\partial p_1}{\partial y})\psi_1(y = 1-\epsilon) - (\frac{\partial p_2}{\partial y})\psi_2(y = 1+\epsilon) = 0 \tag{3.51}$$

for arbitrary smooth test functions ψ_1, ψ_2. This can only mean, $\frac{\partial p_1}{\partial y} = 0$ on Γ_1 and $\frac{\partial p_2}{\partial y} = 0$ on Γ_2.

This case shows that the pressure equations become decoupled in the two subdomains with the fracture being replaced by a no flow boundary condition. This is intuitively consistent with the argument that when the fracture permeability becomes sufficiently small, it acts as a barrier causing breakdown of any communication between the two adjacent subdomains. This is also consistent with the derivation using the analytical approach in first part of this chapter. However, here it is being derived via the dual problem and estimating the flux at the boundaries of the domain in the dual problem.

Case 2, $\beta < 1$

In the first glance, (3.44) seems to pose difficulties since $\epsilon^{\beta-1}$ blows up as ϵ vanishes. However, recall that the energy estimates imply that I_1^ϵ and I_2^ϵ remain bounded. This implies that the

blowing up of the flux term will be balanced by $p_2^\epsilon(y=1+\epsilon) - p_1^\epsilon(y=1-\epsilon)$ which will vanish as $\epsilon \to 0$. In other words $p_2^\epsilon - p_1^\epsilon$ is of order $\epsilon^{1-\beta}$. The first condition is therefore,

$$p_2 = p_1 \text{ at } \Gamma_1.$$

Furthermore, from (3.46) we conclude,

$$(\frac{\partial p_1}{\partial y})\psi_1(y=1-\epsilon) - (\frac{\partial p_2}{\partial y})\psi_2(y=1+\epsilon) = c(\psi_1(y=1-\epsilon) - \psi_2(y=1+\epsilon)) \tag{3.52}$$

leading to the second condition, i.e., the continuity of fluxes at the subdomain interface Γ_1,

$$\frac{\partial p_1}{\partial y} = \frac{\partial p_2}{\partial y} \tag{3.53}$$

Thus, in this case, the fracture does not play any role. The two subdomains are coupled through the interface conditions that include the continuity of pressure and the continuity of fluxes at the interface. This in turn, means that the pressure is continuous. This is once again consistent with the earlier observation using the closed form solution that we had obtained before.

Case 3, $\beta = 1$

Again we will use (3.35) to derive the upscaled model. Let us, as in the previous approach, define

$$\gamma = \frac{y-1}{\epsilon}. \tag{3.54}$$

Introducing this gives us that I_f^ϵ can be rewritten as

$$\epsilon^\beta \frac{\partial p_f^\epsilon}{\partial y} = \epsilon^\beta \frac{\partial p_f^\epsilon}{\partial \gamma}\frac{\partial \gamma}{\partial y} = \epsilon^{\beta-1}\frac{\partial p_f^\epsilon}{\partial \gamma}. \tag{3.55}$$

In terms of this new variable γ the domain $\Omega_f^\epsilon = (1-\epsilon, 1+\epsilon)$ gets mapped to $\Omega_\gamma = (-1,1)$. In terms of γ, Ω_γ, (3.35) gives

$$(\tfrac{dp_1^\epsilon}{dy}, \tfrac{d\psi_1}{dy})_{\Omega_1^\epsilon} \quad + \quad (\tfrac{dp_2^\epsilon}{dy}, \tfrac{d\psi_2}{dy})_{\Omega_2^\epsilon} \quad + \quad (\tfrac{dp_f^\epsilon}{d\gamma}, \tfrac{d\psi_f}{d\gamma})_{\Omega_\gamma} \quad = 0. \tag{3.56}$$

As in the previous cases, choosing the test functions ψ_1 and ψ_2 with compact support we conclude, for the limit of ϵ vanishing, that $-\frac{\partial^2 p_1}{\partial y^2} = 0$ in Ω_1 and $\frac{\partial^2 p_2}{\partial y^2} = 0$ in Ω_2. Similarly as we did earlier ψ_f is chosen with compact support in Ω_γ, to conclude

$$-\frac{\partial^2 p_f^\epsilon}{\partial \gamma^2} = 0 \text{ in } \Omega_\gamma. \tag{3.57}$$

Using this after applying partial integration in all the three terms in (3.56), we obtain

$$\frac{\partial p_1^\epsilon}{\partial y}\psi_1|_{y=1} - \frac{\partial p_2^\epsilon}{\partial y}\psi_2|_{y=1} + \epsilon^{\beta-1}\frac{\partial p_f^\epsilon}{\partial \gamma}\psi_f|_{\gamma=1} - \epsilon^{\beta-1}\frac{\partial p_f}{\partial \gamma}\psi_f|_{\gamma=-1} = 0 \tag{3.58}$$

for arbitrary smooth functions ψ_1, ψ_2, ψ_f. This allows us to conclude, in the limit of ϵ vanishing,

$$\begin{array}{l} \frac{\partial p_1}{\partial y}(y=1) = \frac{\partial p_f}{\partial \gamma} \quad \text{at } \gamma = -1 \\ \frac{\partial p_2}{\partial y}(y=1) = \frac{\partial p_f}{\partial \gamma} \quad \text{at } \gamma = 1 \end{array} \tag{3.59}$$

implying the continuity of fluxes. Furthermore, the continuity of pressures is retained in the limit from the ϵ problem leading to

$$p_1(y=1) = p_f \quad \text{at } \gamma = -1 \tag{3.60}$$

and

$$p_2(y=1) = p_f \quad \text{at } \gamma = 1. \tag{3.61}$$

The upscaled model in this case is identical to the one obtained by closed form solution obtained before. As stated previously, this is a "two scale" model where the fracture domain needs to be scaled to provide the coupling conditions for the subdomains. Thus, what appears as an interface for the two subdomains needs to scaled to an ϵ independent fixed domain in order that the coupling conditions are obtained.

3.3 Summary of the Upscaled Models

For the three cases, $\beta < 1, \beta = 1,$ and $\beta > 1$, we summarise the three upscaled models that we derived above.

1. Case 1: $\beta < 1$ **Average Model**

$$\frac{d^2 p_1}{dy^2} = 0 \text{ in } \Omega_1 \tag{3.62}$$

$$\frac{d^2 p_2}{dy^2} = 0 \text{ in } \Omega_2 \tag{3.63}$$

coupled through the interface conditions,

$$p_1 = p_2 \text{ at } \Gamma_1, \tag{3.64}$$

$$\frac{dp_1}{dy} = \frac{dp_2}{dy} \text{ at } \Gamma_1. \tag{3.65}$$

2. Case 2: $\beta = 1$ **Two-scale Model**
Define, $\Omega_\gamma = (-1, 1)$. The two-scale model is given by

$$\frac{d^2 p_1}{dy^2} = 0 \text{ in } \Omega_1, \tag{3.66}$$

$$\frac{d^2 p_2}{dy^2} = 0 \text{ in } \Omega_2, \tag{3.67}$$

$$\frac{d^2 p_f}{d\gamma^2} = 0 \text{ in } \Omega_\gamma, \tag{3.68}$$

coupled through the interface conditions,

$$\begin{array}{l} \frac{\partial p_1}{\partial y}(y=1) = \frac{\partial p_f}{\partial \gamma} \quad \text{at } \gamma = -1 \\ \frac{\partial p_2}{\partial y}(y=1) = \frac{\partial p_f}{\partial \gamma} \quad \text{at } \gamma = 1 \end{array} \tag{3.69}$$

and

$$p_1(y=1) = p_f \quad \text{at } \gamma = -1 \tag{3.70}$$

and

$$p_2(y=1) = p_f \quad \text{at } \gamma = 1. \tag{3.71}$$

3. Case 3: $\beta > 1$ **Decoupled Model**

$$\frac{d^2 p_1}{dy^2} = 0 \text{ in } \Omega_1 \tag{3.72}$$

$$\frac{d^2 p_2}{dy^2} = 0 \text{ in } \Omega_2 \tag{3.73}$$

and decoupled at the interface by no flow boundary conditions,

$$\frac{dp_1}{dy} = \frac{dp_1}{dy} = 0 \text{ at } \Gamma_1. \tag{3.74}$$

In all these cases, the boundary conditions at $y = 0$ and at $y = 2$ are retained and remain unchanged.

Chapter 4

The Two-Dimensional Case

In this chapter, we consider a two-dimensional problem extending the ideas from the one-dimensional case treated in previous Chapter 3. The idea is again to follow the three steps as in the one-dimensional case. The first step is to define a weak formulation which is standard. This is followed by defining a dual problem that is defined in the fracture domain. The dual problem is a boundary value problem defined in the fracture domain with Dirichlet boundary conditions. This problem isolates the fracture pressure profiles from the subdomains. For this problem, we estimate the fluxes at the fracture/subdomain interfaces. In the final step, we use the estimated fluxes to obtain the limit models that we define as our upscaled model.

As in the one-dimensional case, we have three cases to consider. The fact that we consider only these three cases are not exhaustive. In fact, we apply a periodic boundary conditions on the lateral surfaces (perpendicular to the fracture length). This simplifies the derivation as the integral boundary terms arising due to these surfaces get cancelled. A full discussion including these effects at the fracture vertical boundaries will be a subject of forthcoming paper. Note that in the numerical simulations, we do consider the case when the boundary conditions on the vertical surfaces to the fracture length are Dirichlet and non-periodic.

4.1 The Model Problem

To describe the fracture problem a domain Ω^ϵ like the one in Figure 4.1 is studied. The domain Ω^ϵ is divided into three sub domains. Two larger subdomains, Ω_1^ϵ and Ω_2^ϵ, and one smaller domain Ω_f^ϵ which separates Ω_1^ϵ and Ω_2^ϵ. The domain Ω_f^ϵ is representing the fracture here denoted having the same dimensions but with thickness 2ϵ (Alboin, Jaffré, Roberts, & Serres, 2002). The flow in Ω^ϵ is considered to follow the conservation equation and the Darcy's law relating the gradient of the pressure p^ϵ to the Darcy velocity $\mathbf{u}^\epsilon$:

$$\begin{array}{ll} \nabla \cdot \mathbf{u}^\epsilon = q & \text{in } \Omega^\epsilon \\ \mathbf{u}^\epsilon = -\mathbf{K}\nabla p^\epsilon & \text{in } \Omega^\epsilon \\ p^\epsilon = \bar{p} & \text{on } \partial\Omega^\epsilon. \end{array} \tag{4.1}$$

The superscript ϵ for the unknown variables and the domain emphasises the dependence of them on ϵ. Here p^ϵ is the pressure, $\mathbf{K}$ is the permeability tensor, q is a source term and $\bar{p}$ is the pressure on the boundary $\partial\Omega^\epsilon$. We suppose that K is diagonal. In the two dimensional domain Ω^ϵ, the permeability K can be given as

$$K = \begin{pmatrix} k_{11} & 0 \\ 0 & k_{22} \end{pmatrix} \tag{4.2}$$

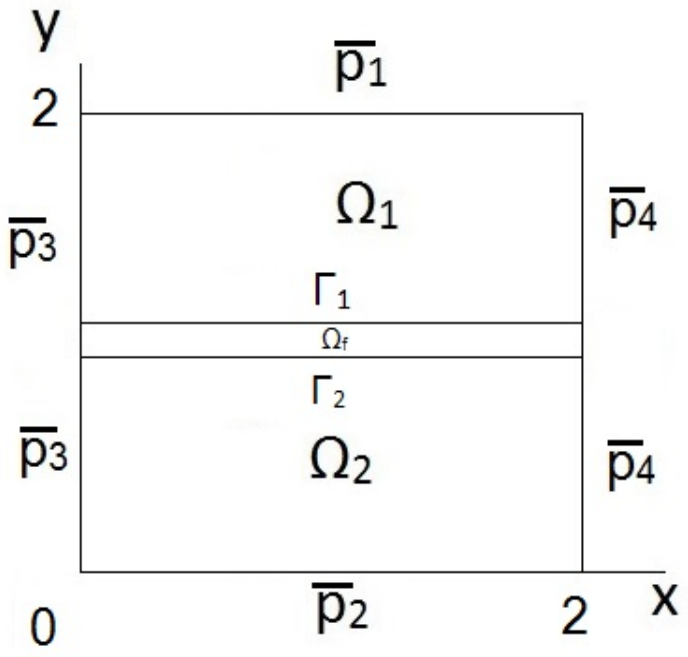

Figure 4.1: The two domains Ω_1 and Ω_1 are separated by the interface Γ with thickness 2ϵ.

where k_{11} and k_{22} are the permeability in horizontal and vertical direction respectively. For simplicity, the permeability in Ω_1^ϵ and Ω_2^ϵ is $k_{11} = k_{22} = 1$. The permeability inside the fracture is taken as $k_{11} = \epsilon^\alpha$ and $k_{22} = \epsilon^\beta$. The extension to other positive definite permeability tensor in the subdomains is straightforward. For the fracture, this remains open as we are strongly using the diagonal structure of this matrix in the fracture.

Let the problem in (4.1) is defined respectively to the domains Ω_i^ϵ where $i = 1, 2, f$, it can be written as

$$\begin{array}{lll} \nabla \cdot \ \mathbf{u}_i^\epsilon = q_i & \text{in } \Omega_i^\epsilon & i = 1, 2, f \\ \mathbf{u}_i^\epsilon = \mathbf{K}_i \nabla p_i^\epsilon & \text{in } \Omega_i^\epsilon & i = 1, 2, f \\ p_i^\epsilon = \bar{p}_i & \text{on } \partial\Omega_i^\epsilon \bigcap \partial\Omega^\epsilon & i = 1, 2 \\ p_i^\epsilon = p_f & \text{on } \Gamma_i^\epsilon & i = 1, 2 \\ \mathbf{u}_i^\epsilon \cdot n_i = \mathbf{u}_f^\epsilon \cdot n & \text{on } \Gamma_i & i = 1, 2 \end{array} \tag{4.3}$$

where n is the normal vector to the fracture, $\Gamma_i^\epsilon = \partial\Omega_i^\epsilon \bigcap \partial\Omega_f^\epsilon \bigcap \Omega^\epsilon$. We assume periodic boundaries on the fracture boundaries at $\partial\Omega_f^\epsilon \bigcap \partial\Omega^\epsilon$, and will denote these boundaries as Γ_3^ϵ at $x = 0$ and Γ_4^ϵ at $x = 2$. The first equation of (4.3) is written out with respect for the three domains and gives us these three equations for the different domains and choose the source terms q_i to be zero.

$$\begin{array}{ll} \frac{\partial^2 p_1^\epsilon}{\partial x^2} + \frac{\partial^2 p_1^\epsilon}{\partial y^2} = 0 & \text{in } \Omega_1^\epsilon, \\ \frac{\partial^2 p_2^\epsilon}{\partial x^2} + \frac{\partial^2 p_2^\epsilon}{\partial y^2} = 0 & \text{in } \Omega_2^\epsilon, \\ \epsilon^\alpha \frac{\partial^2 p_f^\epsilon}{\partial x^2} + \epsilon^\beta \frac{\partial^2 p_f^\epsilon}{\partial y^2} = 0 & \text{in } \Omega_f^\epsilon. \end{array} \tag{4.4}$$

with the outer boundary conditions

$$\begin{array}{rcl} \bar{p}_1 & = & 0, \\ \bar{p}_2 & = & 1, \\ \bar{p}_3 & = & 0, \\ \bar{p}_4 & = & 1, \end{array} \tag{4.5}$$

and the boundaries at the fracture is given as

$$\begin{array}{ll} p_1^\epsilon = p_f^\epsilon & \text{at } \Gamma_1 \\ p_2^\epsilon = p_f^\epsilon & \text{at } \Gamma_2 \\ \frac{\partial p_1^\epsilon}{\partial x} + \frac{\partial p_1^\epsilon}{\partial y} = \epsilon^\alpha \frac{\partial p_f^\epsilon}{\partial x} + \epsilon^\beta \frac{\partial p_f^\epsilon}{\partial y} & \text{at } \Gamma_1 \\ \frac{\partial p_2^\epsilon}{\partial x} + \frac{\partial p_2^\epsilon}{\partial y} = \epsilon^\alpha \frac{\partial p_f^\epsilon}{\partial x} + \epsilon^\beta \frac{\partial p_f^\epsilon}{\partial y} & \text{at } \Gamma_2 \end{array} \tag{4.6}$$

Choosing source term to be zero again simplifies the presentation. Extension to non-zero but independent of ϵ source terms again follows the same arguments.

4.2 A Weak Formulation

A weak formulation for the above model is obtained as in the one-dimensional case. Taking smooth test functions ψ_f defined in Ω_f^ϵ and ψ_1, ψ_2 that have zero boundary values on all the boundaries except the fracture/subdomain interfaces and multiplying the equation in each domain respectively and summing it up gives,

$$-\int_{\Omega_1^\epsilon} \Delta p_1^\epsilon \psi_1 - \int_{\Omega_2^\epsilon} \Delta p_2^\epsilon \psi_2 - \int_{\Omega_f^\epsilon} \nabla \cdot (\mathbf{K}_f^\epsilon \nabla p_f^\epsilon) \psi_f = 0 \tag{4.7}$$

for all smooth test functions ψ_1, ψ_2, ψ_f. Applying partial integration gives

$$\begin{aligned} &\int_{\Omega_1^\epsilon} \nabla p_1^\epsilon \nabla \psi_1 + \int_{\Omega_2^\epsilon} \nabla p_2^\epsilon \nabla \psi_2 + \int_{\Omega_f^\epsilon} \mathbf{K}_f^\epsilon \nabla p_f^\epsilon \nabla \psi_f \\ &- \int_{\partial\Omega_1^\epsilon} (\nabla p_1^\epsilon \cdot n) \psi_1 - \int_{\partial\Omega_2^\epsilon} (\nabla p_2^\epsilon \cdot n) \psi_2 - \int_{\partial\Omega_f^\epsilon} (\mathbf{K}_f^\epsilon \nabla p_f^\epsilon \cdot n) \psi_f = 0 \end{aligned} \tag{4.8}$$

for all smooth test functions ψ_1, ψ_2, ψ_f. On the boundaries $\partial\Omega_i \bigcap \partial\Omega$ for $i = 1, 2$ we have chosen $\psi_1 = \psi_2 = 0$, and we have from (4.6) that

$$\nabla p_1^\epsilon \cdot n = -\mathbf{K}_f^\epsilon \nabla p_f^\epsilon \cdot n \tag{4.9}$$

on the boundary Γ_1 and that

$$\nabla p_2^\epsilon \cdot n = -\mathbf{K}_f^\epsilon \nabla p_f^\epsilon \cdot n \tag{4.10}$$

on Γ_2 which means that the boundary conditions at the interfaces Γ_1 and Γ_2 will cancel each other. For the last boundary conditions Γ_3 and Γ_4 for $x = 0$ and $x = 2$ respectively, we have that

$$\int_{\Gamma_3} (\mathbf{K}_f^\epsilon \nabla p_f^\epsilon \cdot n) \psi_f + \int_{\Gamma_4} (\mathbf{K}_f^\epsilon \nabla p_f^\epsilon \cdot n) \psi_f = -\int_{\Gamma_3} \epsilon^\alpha (\frac{\partial p_f}{\partial x}) \psi_f + \int_{\Gamma_4} \epsilon^\alpha (\frac{\partial p_f}{\partial x}) \psi_f. \tag{4.11}$$

The periodic boundary conditions on Γ_3 and Γ_4 gives that the boundary conditions on Γ_3 and Γ_4 cancel each other. All the boundary terms in (4.8) are cancelled and the equation is reduced to

$$\int_{\Omega_1^\epsilon} \nabla p_1^\epsilon \nabla \psi_1 + \int_{\Omega_2^\epsilon} \nabla p_2^\epsilon \nabla \psi_2 + \int_{\Omega_f^\epsilon} \mathbf{K}_f^\epsilon \nabla p_f^\epsilon \nabla \psi_f = 0 \tag{4.12}$$

for all smooth test functions ψ_1, ψ_2, ψ_f. Now let us define

$$I_f^\epsilon = \int_{\Omega_f^\epsilon} \mathbf{K}_f^\epsilon \nabla p_f^\epsilon \nabla \psi_f \tag{4.13}$$

and further consider this term by applying partial integration once again to get

$$I_f^\epsilon = -\int_{\Omega_f^\epsilon} p_f^\epsilon \nabla \cdot (\mathbf{K}_f^\epsilon \nabla \psi_f) + \int_{\Omega_f^\epsilon} (\mathbf{K}_f^\epsilon \nabla \psi_f \cdot n) p_f^\epsilon \tag{4.14}$$

for all smooth test functions ψ_f. Next, we consider the boundary terms

$$\int_{\Omega_f^\epsilon} (\mathbf{K}_f^\epsilon \nabla \psi_f \cdot n) p_f^\epsilon = \int_{\Gamma_1^\epsilon} \epsilon^\beta (\frac{\partial \psi_f}{\partial y}) p_f^\epsilon - \int_{\Gamma_2^\epsilon} \epsilon^\beta (\frac{\partial \psi_f}{\partial y}) p_f^\epsilon - \int_{\Gamma_3^\epsilon} \epsilon^\alpha (\frac{\partial \psi_f}{\partial x}) p_f^\epsilon + \int_{\Gamma_4^\epsilon} \epsilon^\alpha (\frac{\partial \psi_f}{\partial x}) p_f^\epsilon. \tag{4.15}$$

For a case with periodic boundary conditions at Γ_3^ϵ and Γ_4^ϵ we have that $p_f^\epsilon(x = 0, y) = p_f^\epsilon(x = 2, y)$ where $y \in (1 - \epsilon, 1 + \epsilon)$ and that

$$\frac{\partial \psi_f(x = 0, y)}{\partial x} = \frac{\partial \psi_f(x = 1, y)}{\partial x}. \tag{4.16}$$

This means that the last two boundary terms in (4.15) cancel each other. This motivates the definition of a dual problem. Before the defining this dual problem, as in one-dimensional case, we mention the following results that are immediately obtained by standard techniques of testing with solutions. The above variational form provides us with the following bounds by testing with $\psi_1 = p_1^\epsilon, \psi_2 = p_2^\epsilon, \psi_f = p_f^\epsilon$.

lemma 3. *There exists a $C > 0$ such that $p_1^\epsilon, p_2^\epsilon, p_f^\epsilon$ satisfy the following estimates,*

$$\|\nabla p_1^\epsilon\|^2 + \|\nabla p_2^\epsilon\|^2 + \|\epsilon^\alpha \partial_x p_f^\epsilon\|^2 + \|\epsilon^\beta \partial_y p_f^\epsilon\|^2 \leq C.$$

The above boundedness result readily provides us with the following convergence result.

lemma 4. *There exists p_1, p_2 such that, up to a subsequence, as ϵ goes to zero, $p_1^\epsilon, p_2^\epsilon$ converge to p_1, p_2 weakly in H^1 and thus, strongly in L^2 in their respective domains of definition.*

4.2.1 Dual Problem

Definition 2. Dual problem consists of solving for ξ_f such that

$$\nabla \cdot (K_f^\epsilon \nabla \xi_f) = 0 \text{ in } \Omega_f^\epsilon \tag{4.17}$$

together with the boundary conditions $\xi_f = \psi_1$ and $\xi_f = \psi_2$ on $y = 1 + \epsilon$ and $y = 1 - \epsilon$, respectively and periodic on Γ_3^ϵ and Γ_4^ϵ.

As argued before, for every smooth ψ_f there exists a unique and smooth ξ satisfying the above definition of dual problem. In what follows, we will therefore use ψ_f also to denote the solution of dual problem to reduce the burden of additional unknowns. We can rewrite (4.17) as

$$\frac{\partial}{\partial x}(\epsilon^\alpha \frac{\partial \psi_f}{\partial x}) + \frac{\partial}{\partial y}(\epsilon^\beta \frac{\partial \psi_f}{\partial y}) = 0 \tag{4.18}$$

which becomes

$$\epsilon^\alpha \frac{\partial^2 \psi_f}{\partial x^2} + \epsilon^\beta \frac{\partial^2 \psi_f}{\partial y^2} = 0 \tag{4.19}$$

Next, we resort to a heuristic argument to conclude that the flux satisfies,

$$\|\epsilon^{\beta}\frac{\partial \psi_f}{\partial y}\|_{\infty} \leq C\epsilon^{\beta-1}. \tag{4.20}$$

The heuristic argument is quite straightforward to follow. The test functions ψ_1, ψ_2 are the boundary conditions and are of order $O(1)$. The fracture width is of order ϵ and therefore, the gradient has the scale ϵ^{-1} and multiplying with the factor ϵ^{β} to make it a flux, we get the above estimate. This argument can be made rigorous using maximum principle for the derivative of the above equation with respect to y. This remains outside the scope of this thesis and will be treated in a forthcoming paper based on the results in this thesis.

We can now try to derive an upscaled model and use what we have found so far

$$\int_{\Omega_1^{\epsilon}} \nabla p_1^{\epsilon} \nabla \psi_1 + \int_{\Omega_2^{\epsilon}} \nabla p_2^{\epsilon} \nabla \psi_2 = -I_f^{\epsilon} = -\int_{\Omega_f^{\epsilon}} (\mathbf{K}_f^{\epsilon} \nabla \psi_f \cdot n) p_f^{\epsilon} \tag{4.21}$$

We assume ψ_1 and ψ_2 to have compact support in Ω_1^{ϵ} and Ω_2^{ϵ} which gives that

$$-\nabla \cdot \nabla p_1 = 0 \text{ in } \Omega_1 \quad \text{and} \quad -\nabla \cdot \nabla p_2 = 0 \text{ in } \Omega_2. \tag{4.22}$$

We rewrite the first and the second term in(4.12) as

$$I_1^{\epsilon} = \int_{\Omega_1^{\epsilon}} \nabla p_1^{\epsilon} \nabla \psi_1 = \int_{\Omega_1^{\epsilon}} -\Delta p_1^{\epsilon} \psi_1 + \int_{\partial\Omega_1^{\epsilon}} (\nabla p_1^{\epsilon} \cdot n) \nabla \psi_1 \tag{4.23}$$

and

$$I_2^{\epsilon} = \int_{\Omega_2^{\epsilon}} \nabla p_2^{\epsilon} \nabla \psi_2 = \int_{\Omega_2^{\epsilon}} -\Delta p_2^{\epsilon} \psi_2 + \int_{\partial\Omega_2^{\epsilon}} (\nabla p_2^{\epsilon} \cdot n) \nabla \psi_2 \tag{4.24}$$

which gives that

$$\begin{aligned} I_1^{\epsilon} + I_2^{\epsilon} &= \textstyle\int_{\partial\Omega_1^{\epsilon}} (\nabla p_1^{\epsilon} \cdot n) \nabla \psi_1 + \int_{\partial\Omega_2^{\epsilon}} (\nabla p_2^{\epsilon} \cdot n) \nabla \psi_2 \\ &= -\textstyle\int_{\Gamma_1^{\epsilon}} (\frac{\partial p_1^{\epsilon}}{\partial y}) \psi_1 - \int_{\Gamma_2^{\epsilon}} (\frac{\partial p_2^{\epsilon}}{\partial y}) \psi_2 \\ &= -\textstyle\int_{\Gamma_1^{\epsilon}} \epsilon^{\beta} (\frac{\partial \psi_f}{\partial y}) p_f^{\epsilon} + \int_{\Gamma_2^{\epsilon}} \epsilon^{\beta} (\frac{\partial \psi_f}{\partial y}) p_f^{\epsilon} \end{aligned} \tag{4.25}$$

4.2.2 Case 1, $\beta > 1$

We use the heuristic estimate on the flux term $\epsilon^{\beta}\frac{\partial \psi_f}{\partial y}$ in the last line of (4.34) and obtain that

$$I_1^{\epsilon} + I_2^{\epsilon} = -\int_{\Gamma_1^{\epsilon}} C\epsilon^{\beta-1} p_f^{\epsilon} + \int_{\Gamma_2^{\epsilon}} \epsilon^{\beta-1} p_f^{\epsilon} \to 0 \tag{4.26}$$

as ϵ tends to zero. This gives that

$$= -\int_{\Gamma_1^{\epsilon}} (\frac{\partial p_1^{\epsilon}}{\partial y}) \psi_1 - \int_{\Gamma_2^{\epsilon}} (\frac{\partial p_2^{\epsilon}}{\partial y}) \psi_2 = 0 \tag{4.27}$$

for arbitrary ψ_1 and ψ_2, yielding $\partial_y p_1 = 0$ and $\partial_y p_2 = 0$ at the boundaries Γ_1 and Γ_2. This, the problem becomes decoupled.

4.2.3 Case 2, $\beta = 1$

This case follows closely the derivation in 1D case. We write down the final result directly. Define, $\Omega_{\xi,\eta} = (0,1) \times (-1,1)$. The two-scale model is given by

$$\Delta p_1 = 0 \text{ in } \Omega_1, \tag{4.28}$$
$$\Delta p_2 = 0 \text{ in } \Omega_2, \tag{4.29}$$
$$\Delta_{\xi,\eta} p_f = 0 = 0 \text{ in } \Omega_\gamma, \tag{4.30}$$

coupled through the interface conditions,

$$\begin{array}{l} \frac{\partial p_1}{\partial y}(y=1) = \frac{\partial p_f}{\partial \eta} \quad \text{at } \eta = -1 \\ \frac{\partial p_2}{\partial y}(y=1) = \frac{\partial p_f}{\partial \eta} \quad \text{at } \eta = 1 \end{array} \tag{4.31}$$

and

$$p_1(y=1) = p_f \quad \text{at } \eta = 1 \tag{4.32}$$

and

$$p_2(y=1) = p_f \quad \text{at } \eta = -1. \tag{4.33}$$

4.2.4 Case 3, $\beta < 1$

This case gives rise to the average model currently used a lot in practice. The derivation follows the following arguments, Recall

$$\begin{array}{rl} I_1^\epsilon + I_2^\epsilon & = \int_{\partial\Omega_1^\epsilon} (\nabla p_1^\epsilon \cdot n) \nabla \psi_1 + \int_{\partial\Omega_2^\epsilon} (\nabla p_2^\epsilon \cdot n) \nabla \psi_2 \\ & = -\int_{\Gamma_1^\epsilon} (\frac{\partial p_1^\epsilon}{\partial y}) \psi_1 - \int_{\Gamma_2^\epsilon} (\frac{\partial p_2^\epsilon}{\partial y}) \psi_2 \\ & = -\int_{\Gamma_1^\epsilon} \epsilon^\beta (\frac{\partial \psi_f}{\partial y}) p_f^\epsilon + \int_{\Gamma_2^\epsilon} \epsilon^\beta (\frac{\partial \psi_f}{\partial y}) p_f^\epsilon \end{array} \tag{4.34}$$

Now the estimate on the flux $\epsilon^\beta (\frac{\partial \psi_f}{\partial y}) p_f^\epsilon$ being $O(\epsilon^{\beta-1}$ blows up for this case as ϵ vanishes. At the same time, the energy estimates imply that the integrals $I_i^\epsilon, i = 1, 2$ remain bounded. To counterbalance this blowing up, the pressure p_f^ϵ at $y = 1 \pm \epsilon$ must vanish. This gives the continuity of the pressure.

To obtain condition on the flux, we simply write down the original variational formulation and obtain the strong form providing the relationship between the jump in fluxes and the equation on the fracture line.

Thus, the upscaled model in this case consists of the following problem.

$$-\Delta p_1 = 0 \text{ in } \Omega_1, \tag{4.35}$$
$$-\Delta p_2 = 0 \text{ in } \Omega_2, \tag{4.36}$$
$$\tag{4.37}$$

coupled through the interface conditions,

$$p_1 = p_2 = p_f \text{ at } \Gamma_1, \tag{4.38}$$
$$\frac{\partial p_1}{\partial y} - \frac{\partial p_2}{\partial y} = \frac{d^2 p_f}{d\xi^2} \text{ at } y = 1. \tag{4.39}$$

4.3 Summary of the Upscaled Models

For the three cases, $\beta < 1, \beta = 1,$ and $\beta > 1$, we summarise the three upscaled models that we derived above.

1. Case 1: $\beta > 1$ **Decoupled Model**

$$\Delta p_1 = 0 \text{ in } \Omega_1, \tag{4.40}$$
$$\Delta p_2 = 0 \text{ in } \Omega_2, \tag{4.41}$$
$$\tag{4.42}$$

and decoupled at the interface by no flow boundary conditions,

$$\frac{\partial p_1}{\partial y} = \frac{\partial p_1}{\partial y} = 0 \text{ at } y = 1. \tag{4.43}$$

2. Case 2: $\beta = 1$ **Two-scale Model**
Define, $\Omega_{\xi,\eta} = (0,1) \times (-1,1)$. The two-scale model is given by

$$\Delta p_1 = 0 \text{ in } \Omega_1, \tag{4.44}$$
$$\Delta p_2 = 0 \text{ in } \Omega_2, \tag{4.45}$$
$$\Delta_{\xi,\eta} p_f = 0 = 0 \text{ in } \Omega_\gamma, \tag{4.46}$$

coupled through the interface conditions,

$$\begin{array}{l} \frac{\partial p_1}{\partial y}(y=1) = \frac{\partial p_f}{\partial \eta} \quad \text{at } \eta = -1 \\ \frac{\partial p_2}{\partial y}(y=1) = \frac{\partial p_f}{\partial \eta} \quad \text{at } \eta = 1 \end{array} \tag{4.47}$$

and

$$p_1(y=1) = p_f \quad \text{at } \eta = 1 \tag{4.48}$$

and

$$p_2(y=1) = p_f \quad \text{at } \eta = -1. \tag{4.49}$$

3. Case 3: $\beta < 1$ **Average Model**

$$\Delta p_1 = 0 \text{ in } \Omega_1, \tag{4.50}$$
$$\Delta p_2 = 0 \text{ in } \Omega_2, \tag{4.51}$$
$$\tag{4.52}$$

coupled through the interface conditions,

$$p_1 = p_2 = p_f \text{ at } \Gamma_1, \tag{4.53}$$
$$\frac{\partial p_1}{\partial y} - \frac{\partial p_2}{\partial y} = \frac{d^2 p_f}{d\xi^2} \text{ at } y = 1. \tag{4.54}$$

In all these cases, the boundary conditions at the outer boundaries of Ω are retained and remain unchanged.

Chapter 5

Numerical Methods

To solve the problem described in the two previous chapters we have used MATLAB Reservoir Simulation Toolbox (MRST), which is an open source code developed by SINTEF (Lie et al., 2012). This MATLAB based toolbox is used to calculate the pressure distribution in the domain Ω. The two-dimensional domain Ω is discretized, which means that the domain is split up into a finite number of non-overlapping subdomains Ω_{ij} (Anderson & Wendt, 1995). Each subdomain or grid cell is associated with with a certain number of variables, which is determined when the system is solved. For a simple one-dimensional problem this can easily be done by analytical solutions, as in (Nordbotten & Celia, 2012) but already for 2D, closed form solutions are out of reach and with increase in the complexity of the problem we resort to computer based tools and numerical approximations. For the two-dimensional case, the flux and pressure distribution are solved for each domain Ω_1, Ω_2 and Ω_f separately applying a two point flux model which is described in 5.0.1. This is again done using MRST. The software contains several toolboxes for performing computations using a variety of meshes and equations applicable to the reservoir modelling and simulations. The software contains a wide range of data structures and computational methods that can be used to make custom made modelling tools. We use standard cell centred finite volume method, that is, we use two point flux approximation with cell centred unknowns for the pressure with the fluxes being defined at the edges. The standard mixed method with RT_0 elements yields identical approach for the rectangular mesh that we have considered. We take rectangular grid cells to mesh a 2D rectangular domain and the MRST calculates the pressure in every cell and the flux through every cell interface. in accordance with the different cases derived in Chapter 3 and Chapter 4 we have imposed different boundary conditions on the fracture interface.

5.0.1 The Two Point Flux Approximation

The two point flux approximation is used on the the pressure equation (5.1) to find the flux over each cell interface.

$$\nabla \cdot (-\mathbf{K}\nabla p) = q. \tag{5.1}$$

As described in the theory, this is the pressure equation for a isotherm single phase system with constant density where the gravity forces are neglected. To find the pressure, (5.1) is integrated over every single cell Ω_{ij} and then the divergence theorem is used to obtain

$$\int_{\partial\Omega_{ii}} \mathbf{K}\nabla p \cdot \mathbf{n} dS = \int_{\Omega_{ii}} q \; d\Omega, \tag{5.2}$$

where n is the outward unit normal vector. Equation (5.2) is known as the conservation law. By using (5.2), the flux over each cell interface can be approximated by the pressure in each

neighbouring cell.

$$q_{\Gamma_{ik}} \int_{\partial\Gamma_{ik}} \mathbf{K}\nabla p \cdot \mathbf{n} dS \approx \sum_{j=1}^{v} T_j p_j, \quad \Gamma_{ik} = \Omega_i \bigcap \Omega_k, \tag{5.3}$$

where T_j is the contribution from cell j, and v is the number of nearby cells. The pressure at

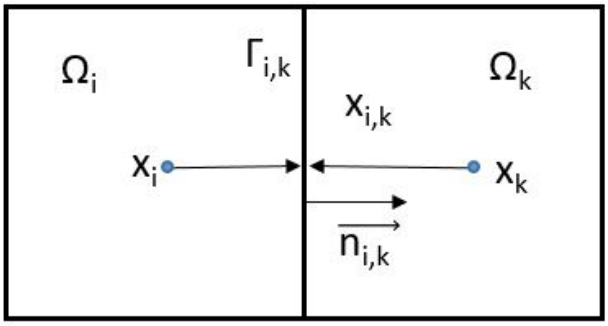

Figure 5.1: A two point flux discretization for grid cells Ω_i and Ω_k

$x_{i,k}$ is assumed to be the average of the pressure in x_i and x_k, and the flux from Ω_i to Ω_k can be found by

$$q_{ik} = -\int_{\partial\Gamma_{ik}} \overrightarrow{n_{ik}} \cdot (\mathbf{K}_i \nabla p)\ dS \approx a_{ik}(p_i - p_{ik}), \tag{5.4}$$

where

$$a_{ik} = \frac{A_{i,k}\overrightarrow{n_{i,k}} \cdot \mathbf{K}_i}{d_{i,k} \cdot d_{i,k}}. \tag{5.5}$$

Here $A_{i,k}$ is the area over the shared surface, $d_{i,k}$ the distance from the center of the cell to the interface and $\mathbf{K}_i$ the permeability in the cell Ω_i. The expression for the flux from Ω_k to Ω_i is given by

$$q_{ki} = -\int_{\partial\Gamma_{ki}} \overrightarrow{n_{ki}} \cdot (\mathbf{K}_k \nabla p)\ dS \approx a_{ki}(p_k - p_{ki}). \tag{5.6}$$

From (5.4) and (5.6) we have that

$$a_{ik}^{-1} q_{ik} = p_i - p_{ik} \quad and \quad a_{ki}^{-1} q_{ki} = p_k - p_{ki}. \tag{5.7}$$

The pressure at the interface between two cells is defined such that $p_{ki} = p_{ik}$. This will give from (5.7) that

$$a_{ik}^{-1} q_{ik} - a_{ki}^{-1} q_{ki} = p_i - p_k. \tag{5.8}$$

The fluxes q_{ik} and q_{ki} are on the same interface, which means that they have to be equal but with different signs,

$$q_{ik} = -q_{ki}. \tag{5.9}$$

Taking this into account we can rewrite (5.8) such that

$$[a_{ik}^{-1} + a_{ki}^{-1}] q_{ik} = p_i - p_k, \tag{5.10}$$

and then obtain the flux over one interface by rearranging the equation into

$$q_{ik} = [a_{ik}^{-1} + a_{ki}^{-1}]^{-1}(p_i - p_k), \tag{5.11}$$

This flux term can be inserted into the pressure equation (5.1) which then give

$$\sum_{k=1}^{n_i} q_{ik} = [a_{ik}^{-1} + a_{ki}^{-1}]^{-1}(p_i - p_k) = q \quad \text{all } \Omega_i \subset \Omega \quad i = 1, ..., n. \tag{5.12}$$

where n_i is the face number for the cell Ω_i and n is the total number of cells (Lie, 2015). This equation can easily be solved and used to plot a pressure for a simple domain. In a fractured

medium there may not be an easy way to find the flux at every interface. The fracture size or the sudden change of permeability may give an unconformity of the flux, and this has to be taken into account when solving the problem. For the simulations in this model we will calculate the jump in flux over a fracture with three different models. The models represent the three different cases found in Chapter 3.

5.1 Numerical Models

There are three different models in Chapter 3 and Chapter 4 that are studied. The quality of each model is considered with respect to the values of α and β, similar to the derivation using the weak solutions. One model where we have a linear profile, one where there is a discontinuity of the pressure at the fracture interfaces but the fracture pressure profile connects the discontinuities and one where the fracture can be treated as a no flow boundary condition. The three models are all tested against an epsilon model which serves as the reference solution. In the Epsilon model, we resolve the fracture explicitly.

5.1.1 The Average Model

This model is working for $\beta < 1$ and we call it the average model because the fracture pressure basically is the average of the surrounding pressures. The interfaces Γ_1 and Γ is given Dirichlet boundary conditions calculated in the fracture. The fracture is considered as a thin domain

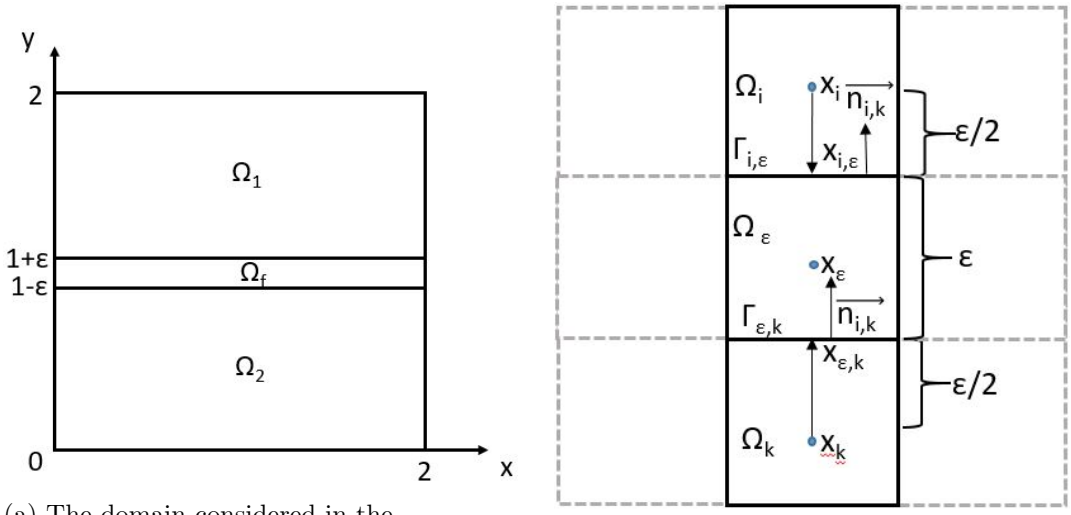

(a) The domain considered in the epsilon model.

(b) The interface between a single grid block of Ω_1, Ω_ϵ and Ω_2.

Figure 5.2: The separation of the domain which is done to solve for the average model.

Ω_f with thickness of one grid cell like shown in Figure5.2a. In Figure 5.2b one grid block Ω_ϵ is considered. The pressure in the middle of the grid is set to be the average of the pressures in x_i and x_k. The pressures conditions on the interfaces $x_{i,\epsilon}$ and $x_{\epsilon,k}$ will become equal to the pressure in Ω_ϵ.

5.1.2 The Two Scaled Model

In this model the fracture is considered as a separate domain, Ω_f, as shown in Figure 5.3. The domains Ω_1 and Ω_2 are first solved separately using the pressure conditions imposed on the sides of the domains, then the flux calculated to leave Ω_1 and Ω_2 through the interfaces Γ_1 and Γ_2 is used as the Neumann boundary conditions on the top and bottom interfaces of Ω_f. This

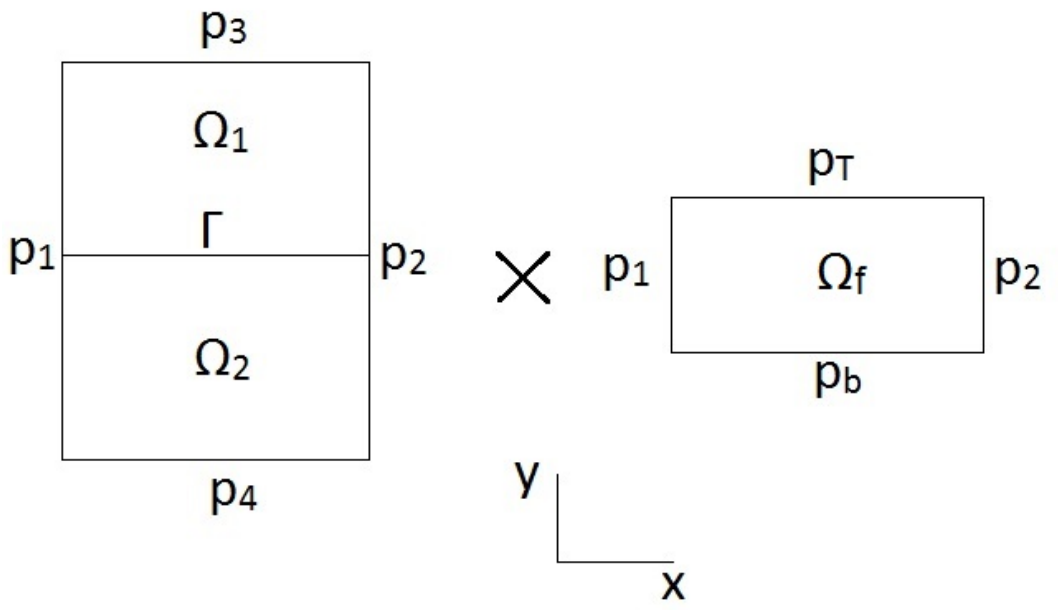

Figure 5.3: The domains Ω_1 and Ω_2 are separated by a layer γ, which is called γ_1 or γ_2 depending of the side of the interface. In the numerical models the interface conditions are calculated using the domain Ω_f

domain represents the fracture and is described like the domain derived in Chapter 3 for case 4, and the flux and pressure problem can be described like

$$\frac{\partial^2 p_f^\epsilon}{\partial x^2} + \frac{\partial^2 p_f^\epsilon}{\partial \gamma^2} = 0, \tag{5.13}$$

for a one-dimensional case, and like

$$k_{xx}\frac{\partial^2 p_f^\epsilon}{\partial x^2} + \frac{\partial^2 p_f^\epsilon}{\partial \gamma^2} = 0 \tag{5.14}$$

for a two-dimensional case. Here $\gamma = \frac{1-y}{\epsilon}$ like in Chapter 3 for the cases where $\beta = 1$, and k_{xx} is the permeability in the x-direction. This problem is solved a few times and the boundary conditions are updated for each iteration. This is a standard domain decomposition approach for solving this model.

5.1.3 The Decoupled Model

This is a model for fractures where the permeability in the y-direction is characterised by $\beta > 1$. The two layers at each side of the fracture is treated as two decoupled domains separated by an aquitard or barrier. The domains Ω_1 and Ω_2 are solved separately with a no flow boundary condition at the fracture interface and Dirichlet condition at the other sides of the domains.

5.1.4 The Epsilon Model

The epsilon model is given the name because the fracture thickness is represented by the size ϵ. The domain considered in this model is of size $\Omega_1 + \Omega_f + \Omega_2$, where the permeability is specified in each grid cell of the domain. The grid cells on the location of the fracture is given the permeability if the fracture. The model is solved applying the TPFA solver included in

MRST. The results from the epsilon model gives a basic idea of how the medium would look like if it was a homogeneous domain where the only change was the permeability. This model is used as the reference model for the other cases.

5.1.5 Error Estimates

There are two types of error that are calculated in the results. The first one is the pressure error which is used to find the error for a certain x-value, usually for $x = 1$ in the one-dimensional case. The error is plotted with respect to y. This is done by taking the absolute pressure difference between the specific fracture model and the reference model (epsilon model).

$$\text{Error} = \frac{|p_i - p_{ref}|}{.} \tag{5.15}$$

To find the relative domain error in the domain for different values of α and β we have applied the Euclidean norm (Kincaid & Cheney, 2002). The square of the pressure difference between the two models are summed together for all grid blocks in the domain, divided by the sum of the pressure in the reference model and then taken the square root of.

$$\text{Domain error} = \sqrt{\frac{\sum_{n=1}^{N}(p_i - p_{ref})^2}{\sum_{n=1}^{N} p_{ref}^2}} \tag{5.16}$$

This error is plotted for different values of α and β to show where the different models are good approximations or not.

Chapter 6

Simulation Results

In this chapter, we present the numerical simulation of both the reference problem and the different upscaled models obtained in Chapters 3 and 4. The problem that we solve numerically remains the same as the one analysed before in these chapters. That is, we consider a single phase flow in a 2D geometry without including the effects of gravity. At the risk of repetition, we recall once again the model problem, (see also 4)

$$\begin{aligned} \text{div } \mathbf{u} &= 0 \quad \text{in } \Omega \\ \mathbf{u} &= -\mathbf{K}\nabla p \quad \text{in } \Omega \end{aligned} \tag{6.1}$$

where the domain is the same as in Figure 4.1. For the boundary conditions, we will use the Dirichlet boundary conditions for all the boundaries. Note that this is in contrast with the theoretical discussions in Chapter 4, Section 4 where we assumed periodic boundary conditions for the fracture lateral surfaces. The width of the fracture in all our simulations is given as $\epsilon = \frac{2}{500}$ unless it is otherwise specified. In accordance with the theoretical discussions, we begin with the one-dimensional case.

6.1 One-Dimensional Case

We retain the 2D geometry for also studying the 1D problem and simply adapt the boundary conditions in such a way that the problem becomes pseudo 1D. Specifically, we take no flow boundary conditions on the sides of the domain parallel to the y-axis. The boundary conditions at the top of the domain is $p_1 = 0$, and at the bottom $p_2 = 1$. For the sides there are no flow boundary conditions. The problem is solved with the models described in the previous chapter for different values of β and compared to the reference solution.

For all the three upscaled models, we study the accuracy of this model for different values of β. In particular, we also study the validity of approximation outside the validity range of this model. We then show the error behaviour corresponding to different values of β. we refer to Section 4.3 for the summary of these upscaled models obtained for different values of β. Just to recall, we once again present the upscaled models here.

For the three cases, $\beta < 1, \beta = 1$, and $\beta > 1$, we summarise the three upscaled models that we derived above. Recall that for the boundary conditions taken above, this pseudo 1D problem has solutions p_1, p_2, p_f only depending upon y and are independent of x. This justifies the ordinary derivatives below. As we will see later, in 2D case, we will retain the partial derivatives replacing the ordinary derivatives. Interestingly, the 2D upscaled model also has the same structure.

1. Case 1: $\beta < 1$ **Average Model**

$$\frac{d^2 p_1}{dy^2} = 0 \text{ in } \Omega_1, \tag{6.2}$$

$$\frac{d^2 p_2}{dy^2} = 0 \text{ in } \Omega_2 \tag{6.3}$$

coupled through the interface conditions,

$$p_1 = p_2 \text{ at } \Gamma_1, \tag{6.4}$$

$$\frac{dp_1}{dy} = \frac{dp_2}{dy} \text{ at } \Gamma_1. \tag{6.5}$$

2. Case 2: $\beta = 1$ **Two-scale Model**
Define, $\Omega_\gamma = (-1, 1)$. The two-scale model is given by

$$\frac{d^2 p_1}{dy^2} = 0 \text{ in } \Omega_1, \tag{6.6}$$

$$\frac{d^2 p_2}{dy^2} = 0 \text{ in } \Omega_2, \tag{6.7}$$

$$\frac{d^2 p_f}{d\gamma^2} = 0 \text{ in } \Omega_\gamma, \tag{6.8}$$

coupled through the interface conditions,

$$\begin{array}{l} \frac{\partial p_1}{\partial y}(y=1) = \frac{\partial p_f}{\partial \gamma} \quad \text{at } \gamma = -1 \\ \frac{\partial p_2}{\partial y}(y=1) = \frac{\partial p_f}{\partial \gamma} \quad \text{at } \gamma = 1 \end{array} \tag{6.9}$$

and

$$p_1(y=1) = p_f \quad \text{at } \gamma = -1 \tag{6.10}$$

and

$$p_2(y=1) = p_f \quad \text{at } \gamma = 1. \tag{6.11}$$

3. Case 3: $\beta > 1$ **Decoupled Model**

$$\frac{d^2 p_1}{dy^2} = 0 \text{ in } \Omega_1 \tag{6.12}$$

$$\frac{d^2 p_2}{dy^2} = 0 \text{ in } \Omega_2 \tag{6.13}$$

and decoupled at the interface by no flow boundary conditions,

$$\frac{dp_1}{dy} = \frac{dp_1}{dy} = 0 \text{ at } \Gamma_1. \tag{6.14}$$

In all these cases, the boundary conditions at $y = 0$ and at $y = 2$ are retained and remain unchanged.

6.1.1 The Average Model

We consider the following cases:

1. We take $\beta = -0.5$ and compute the pressure profile using the Average Model. We obtain the expected linear profile for pressure. See Figure 6.1.
2. We choose $\beta = 0.5$ and solve both the full model, that is, the reference Epsilon model and the upscaled model. We compare the accuracy of the solution and behaviour of the error. (See Figure 6.2)
3. For $\beta = 1.1$, we again compute both the reference solution and the Average model solution. We compare the error for this case. Note that this value of β is outside the validity range of the upscaled model. (See Figure 6.2)
4. Finally, we choose a range of β values and show the behaviour of the error with respect to the reference Epsilon model (See Figure 6.3).

First, the problem is solved with the average model for $\beta = -0.5$ and the pressure is plotted in Figure 6.1a. The pressure change is linear from $y = 0$ to $y = 2$, and the pressure remains independent of x. This is shown in Figure 6.1b where the pressure is plotted for $p(0.4, y)$, $p(1, y)$ and $p(1.6, y)$. In Figure 6.2, the pressure calculated with the Average model is compared with the Epsilon model for different values of β to study the pressure difference calculated using the two models.

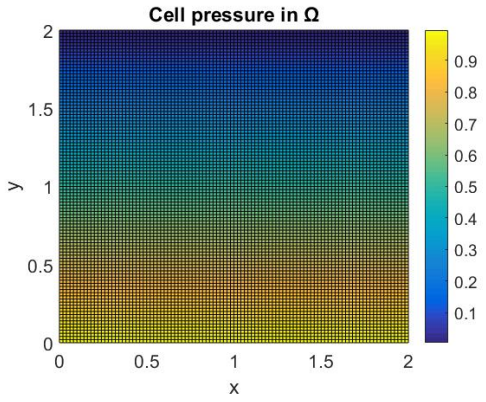

(a) Pressure profile of the domain Ω with $\beta = -0.5$.

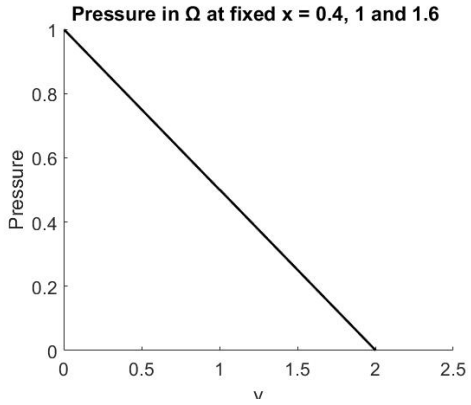

(b) Pressure cange with respect to y at x=0.4, 1 and 1.6.

Figure 6.1: The two plots show the pressure distribution for the whole domain (a) and for different values of x. The pressures for $x = 0.4$, 1 and 1.6 is shown in (b). The plots at different locations for x confirm that the pressure remains independent of x-values.

The plots in In Figure 6.2a and Figure 6.2c, where the pressure is plotted against the y-value for both the average model and the epsilon model, shows that there is a little error in the pressure when $\beta < 1$, showing a good agreement between the upscaled model and the reference model. The pressure difference in the two models increases as the value of β becomes larger. This is as expected considering the calculations in Chapter 3. The plots in Figure 6.2e and Figure 6.2f, gives the pressure and error for a case where we do not expect the model to work. This is when β is larger than 1. A different model should be considered as the average model no longer suits as a good approximation. The relative domain error is calculated in Figure 6.6

From the above plots, we make the following conclusions.

6.1.2 Conclusions

1. For the case $\beta = -0.5$ the Average model shows the expected linear profile for pressure as shown in Figure 6.1. This case is within the validity range of $\beta < 1$ for which the Averaged model is derived.

2. For $\beta = 0.5$, the reference Epsilon model and the upscaled model show a good agreement. Also, the error shows that it is maximum at the fracture location and gradually reduces as we move away from the fracture interface. Within the subdomains, the errors are likely to be less if the regions near the fracture interfaces are discounted. These results are shown in the Figures 6.2. Furthermore, we also see that the approximation improves for $\beta = -0.5$. Thus, the Averaged model provides an improved approximation as we take lower values of β.

3. For $\beta = 1.1$ lies outside the validity range of this model. For this case, we see that the matching between the reference solution and Average model is quite poor suggesting that this is no longer a useful approximation for the reference model. This further strengthens the argument that the upscaled models have a definite range of validity outside which they perform quite poorly. These results are shown in Figure 6.2.

4. Finally, we choose a range of β values and show the behaviour of the error with respect to the reference Epsilon model (See Figure 6.3). We observe that as β increases, the approximation quality of this model reduces drastically. Especially, outside the range of validity, the approximation quality is already unacceptable. At the same time, within the validity range, this provides a good agreement with the quality of upscaling improving as we reduce the value of β.

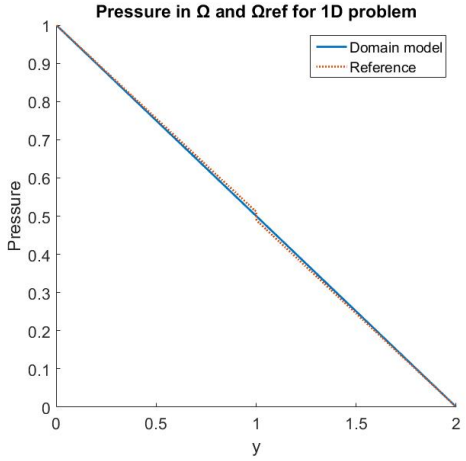

(a) Pressure for $\beta = 0.5$. The pressure is plotted for both the average model and the epsilon model.

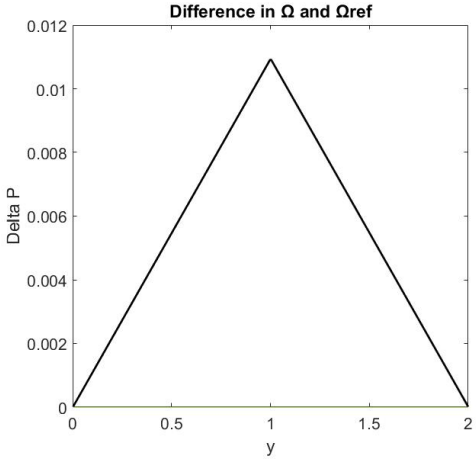

(b) This figure shows the difference in pressure between the average model and the epsilon model for $\beta = 0.5$.

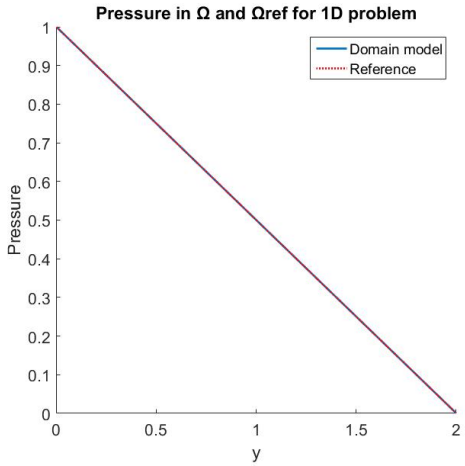

(c) Pressure for $\beta = -0.5$. The pressure is plotted for both the average model and the epsilon model.

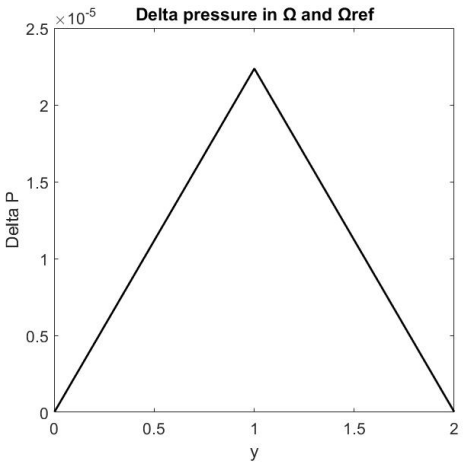

(d) This figure shows the difference in pressure between the average model and the epsilon model for $\beta = -0.5$.

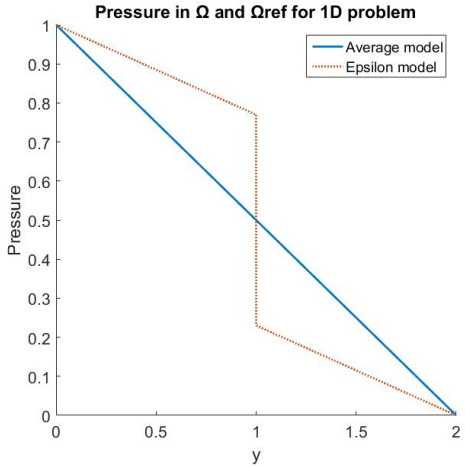

(e) Pressure for $\beta = 1.1$. The pressure is plotted for both the average model and the epsilon model.

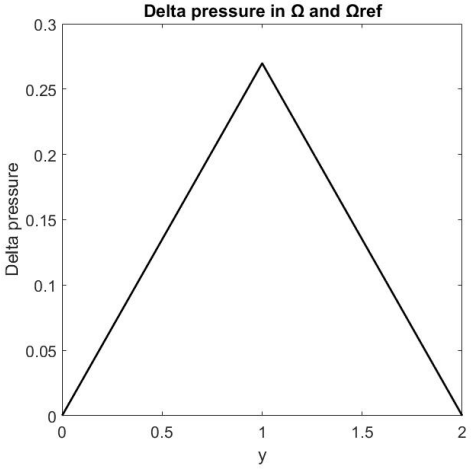

(f) Difference in pressure between the average model and the epsilon model for $\beta = 1.1$.

Figure 6.2: Pressure plots for two different values of β.

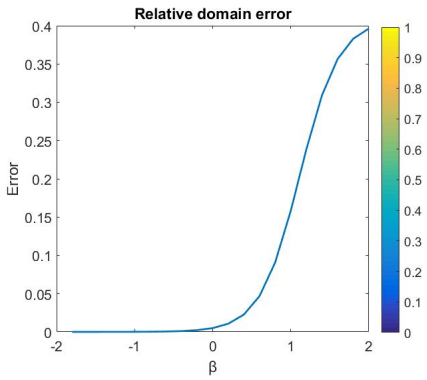

Figure 6.3: The domain error for the average model using the euclidean norm given for different values of β. The error is computed with respect to the reference solution

6.1.3 The Two Scale Model

We consider the following cases

1. We take $\beta = 1$ and compute the pressure profile using the Two Scaled Model and the reference Epsilon model. We compare the accuracy of the solution and behaviour of the error. (See Figure 6.5)

2. We chose $\beta = 1.5$ and again solve the full model, which is both the Two Scaled Model and the reference Epsilon Model. We compare the error for this case. Note that β is to large, and that we are outside the validity range of the upscaled model. (See Figure 6.5)

3. We chose $\beta = 0.5$ and again solve the full model. We compare the error for this case. In this case β is to small, and we are again outside the validity range of the upscaled model. (See Figure 6.5)

4. Finally, we choose a range of β values and show the behaviour of the error with respect to the reference Epsilon model (see Figure 6.6).

The two scaled model is assumed to be a good approximation for $\beta = 1$. The model is tested for $\beta = 1$ and the pressure in plotted in Figure 6.4. The plot shows that most if the pressure change happens in the fracture, but some of it occurs in Ω_1 and Ω_2.

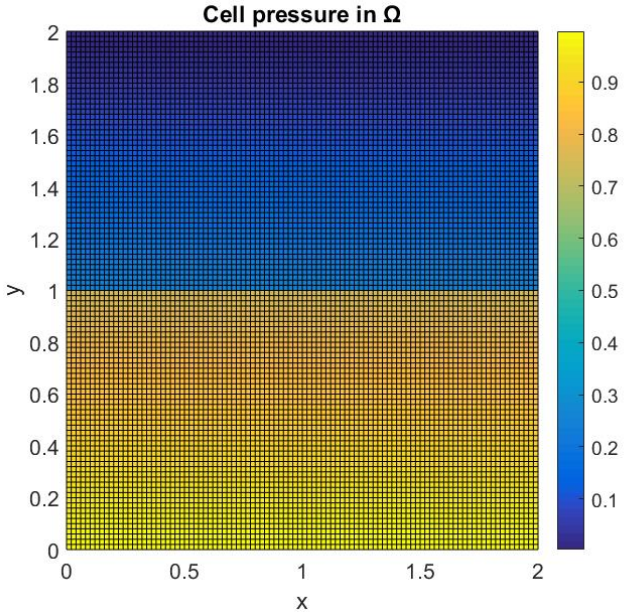

Figure 6.4: The pressure is plotted with respect to x and y for $\beta = 1$.

We have from 6.5a and 6.5b that the model can be used as an approximation for $\beta = 1$ and from the other plots in Figure 6.5 that it is not a good model for $\beta = 1.5$ or $\beta = 0.5$. The domain error for the model is plotted with respect to β in Figure 6.6 using the Euclidean norm.

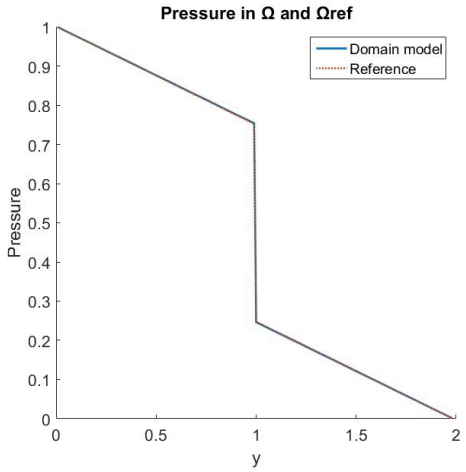

(a) Pressure for $\beta = 1$.

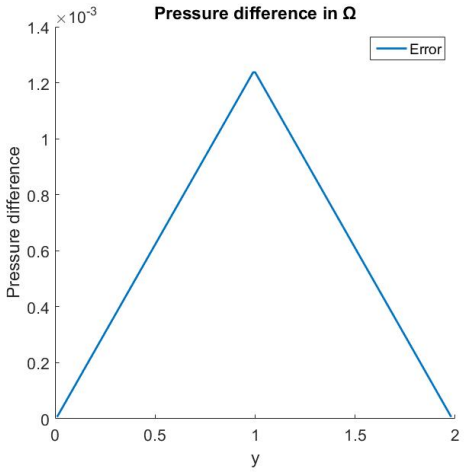

(b) Pressure difference for $\beta = 1$.

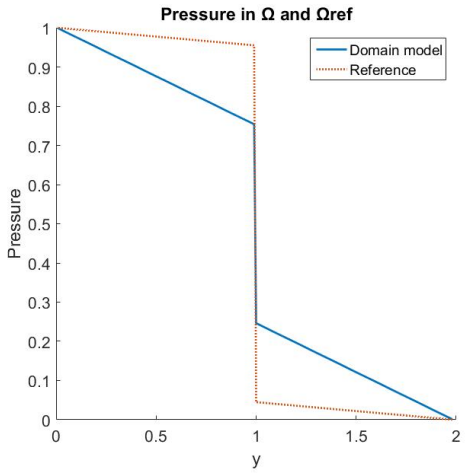

(c) Pressure for $\beta = 1.5$.

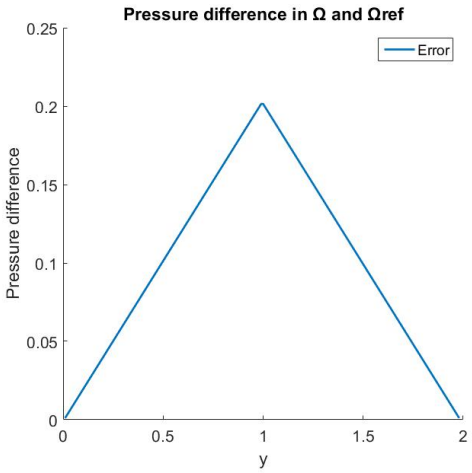

(d) Pressure difference for $\beta = 1.5$.

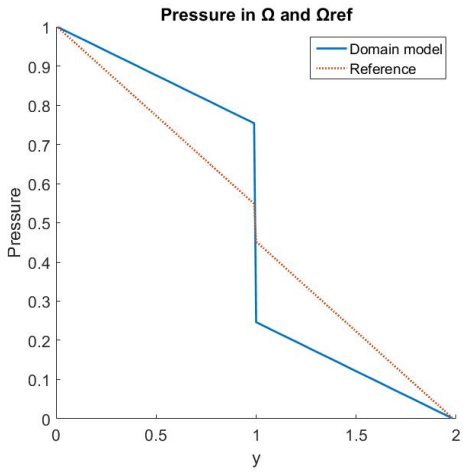

(e) Pressure for $\beta = 0.5$.

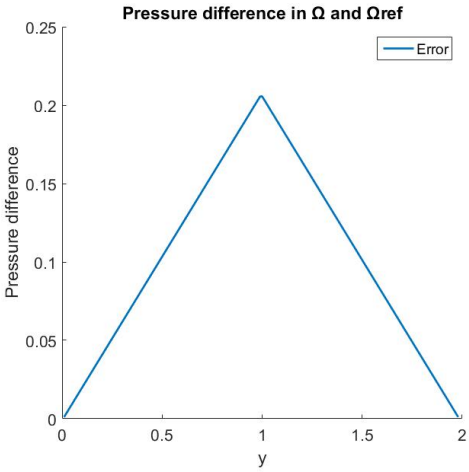

(f) Pressure difference for $\beta = 0.5$.

Figure 6.5: The pressure given by the two scaled model is plotted and compared with the pressure given by the epsilon model.

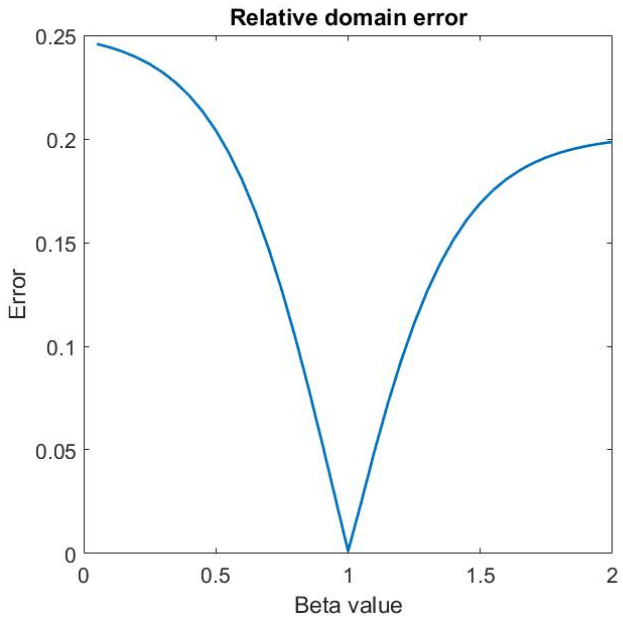

Figure 6.6: The domain error for different values of β, for the two scaled model. The error is calculated using the euclidean norm and with respect to the reference solution.

6.1.4 Conclusion

1. For the case $\beta = 1$ the Two Scaled Model shows that there is a pressure change inside and outside of the fracture as expected. This case is inside the validity of the upscaled model (See Figure 6.5).

2. For $\beta = 1.5$ we see that the Two Scaled Model and the reference Epsilon Model matches poorly. The model in no good as an approximation in this case. (See Figure 6.5)

3. For the case $\beta = 0.5$ we are again outside the validity range of the upscaled model. This shows that the validity range of this model is limited. (See Figure 6.5)

4. Finally, we choose a range of β values and show the behaviour of the error with respect to the reference Epsilon model (see Figure 6.6). We observe that the approximation quality of this model increases as the value of β approaches 1. Within validity range however, this model can provide as an good upscaled model.

6.1.5 The Decoupled Model

We consider the following cases

1. We take $\beta = 2$ and compute the pressure profile using the Decoupled Model and the reference Epsilon model. We compare the accuracy of the solution and behaviour of the error, and see that we obtain an expected decoupled pressure profile (See Figure 6.7).

2. We do again chose $\beta = 2$, and this time we reduce the size of the fracture 100 times. We solve for both the Decoupled Model and the reference Epsilon model, and plot the error (see Figure 6.8).

3. We compare the errors obtained for $\beta = 2$ for different sizes of epsilon and plots the difference in Figure 6.9b.

4. Finally, we choose a range of β values and show the behaviour of the error with respect to the reference Epsilon model (see Figure 6.10).

The calculations in Chapter 3 showed that the fracture acts as an barrier $\beta > 1$. There is no information going trough the fracture, and the domain becomes decoupled. In Figure 6.7, the pressure is solved with the decoupled model for $\beta = 2$ and plotted with respect to x and y.The top half takes the boundary pressure from the top and distributes this to the domain, and the bottom half takes the pressure from the bottom boundary pressure which is given to the bottom half of the domain.

The plots in Figure 6.8 shows that there is a small difference in the pressure between the decoupled model and the epsilon model for $\beta = 2$. The way of decoupling the domains can be justified. The plots in Figure 6.8c and Figure 6.8d shows that the error of the model decreases when the grids cells becomes smaller. By decreasing the grid size by a hundred times the pressure difference becomes a hundred times smaller. By reducing the grid size, the fracture becomes thinner, while the permeability in the fracture decreases, and the reference model gives a more decoupled pressure profile. The error difference shown in Figure 6.9 is calculated using this formula

$$E(y) = \frac{\Delta p_{100}(y)}{\Delta p(y)} \tag{6.15}$$

where p is the pressure in the first calculation, and p_{100} is the pressure when the grid size is hundred times smaller. The relative domain error for the decoupled model is plotted in Figure 6.10. This shows that the model can be used for $\beta > 1$ as long as $\epsilon \to 0$

6.1.6 Conclusion

1. For the case $\beta = 2$ the Decoupled Model shows that decoupled pressure profile is a valid approximation for this case (See Figure 6.7).

2. By reducing the size of the fracture 100 times we see that the error is reduced 100 times. The grid size does have a larg effect on the errors that we approximate (see Figure 6.9b).

3. Finally, we choose a range of β values and show the behaviour of the error with respect to the reference Epsilon model (see Figure 6.10). We observe that the model is a good approximation, and that it has validity when $\beta > 1$

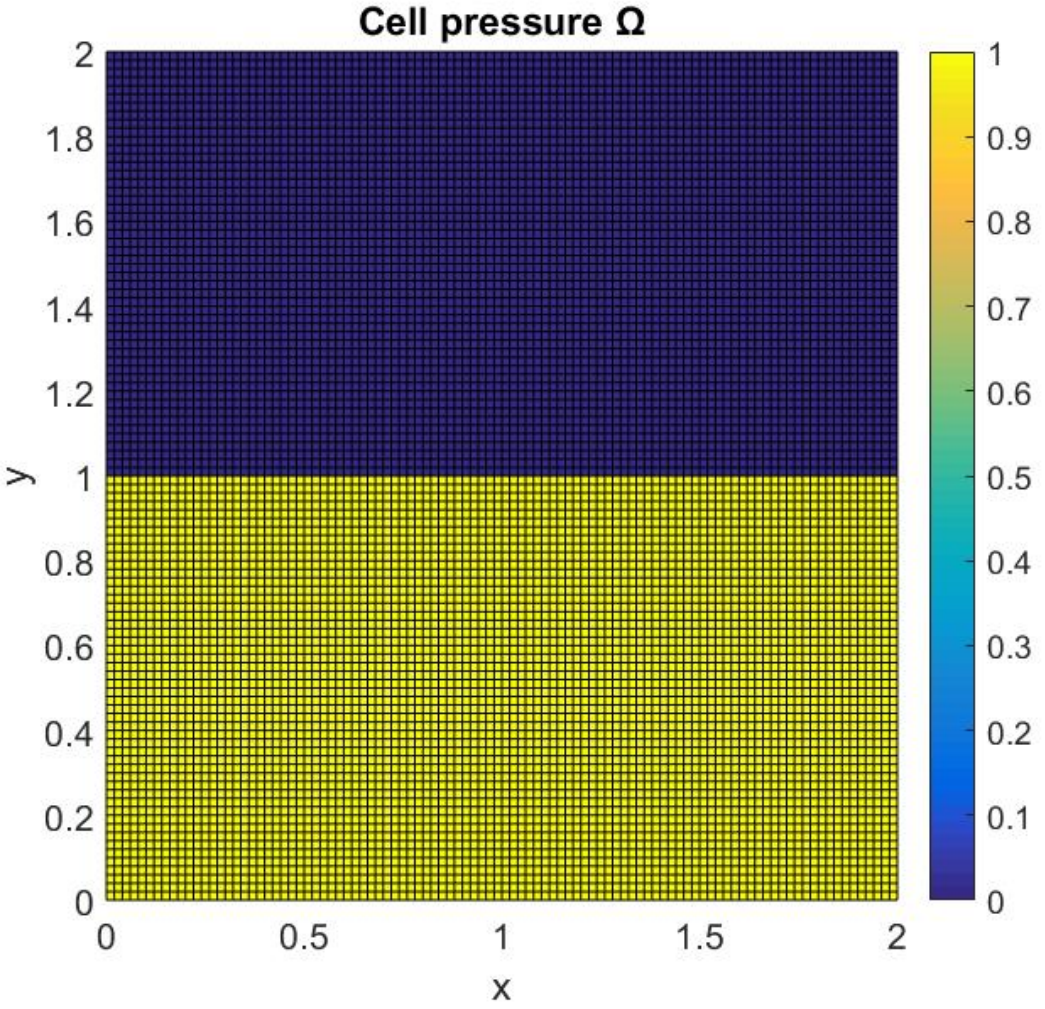

Figure 6.7: The figure shows the pressure distribution in Ω for a decoupled problem like we have when $\beta = 2$.

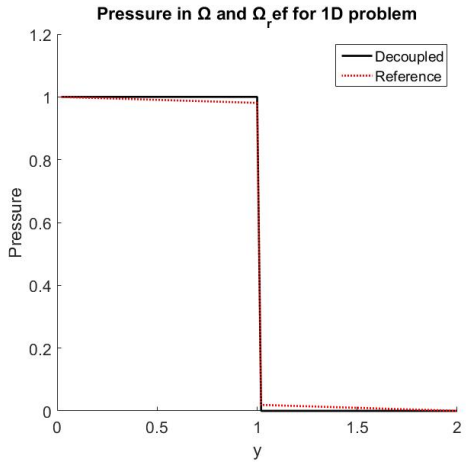

(a) The pressure in the domain for a decoupled problem for $\beta = 2$.

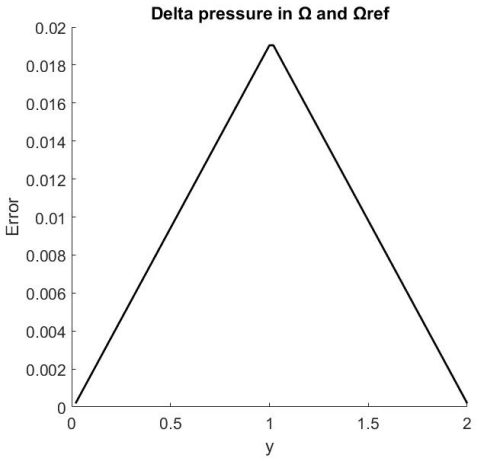

(b) The pressure difference between the decoupled problem and the reference problem.

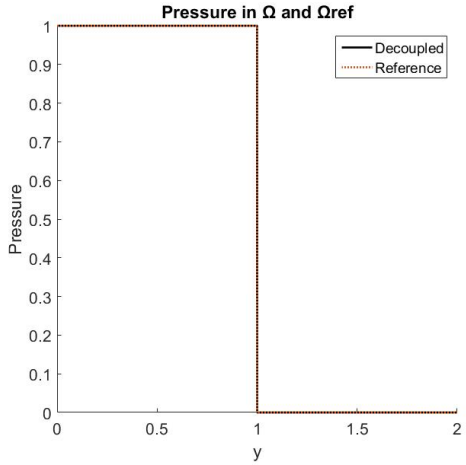

(c) The pressure in the domain for a decoupled problem with $\beta = 2$ with grid size a 100 times smaller than in 6.8a.

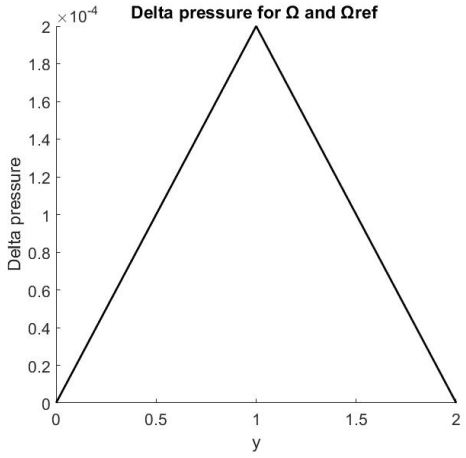

(d) The difference between the decoupled problem and the reference problem with grid size a 100 times smaller than in 6.8b.

Figure 6.8: The figures show the pressure in Ω using the decoupled method, and the difference between the decoupled method and the epsilon method. The figures does also show the affect the grid size has on the difference between the average and the epsilon model.

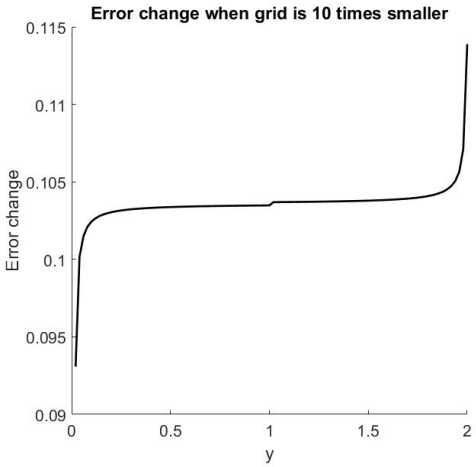

(a) The change in pressure when the grid size becomes 10 times smaller.

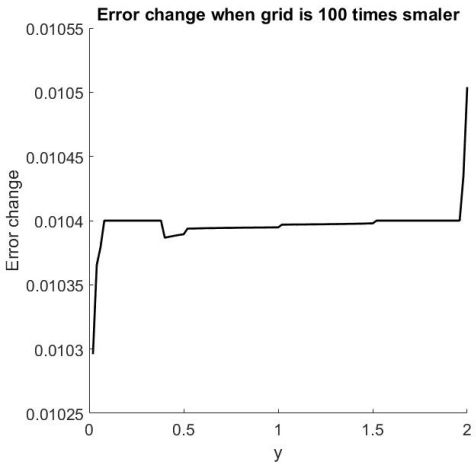

(b) The change in pressure when the grid size becomes 100 times smaller.

Figure 6.9: The two figures show how the pressure difference in the decupled model and the epsilon model becomes smaller when the grid size is reduced.

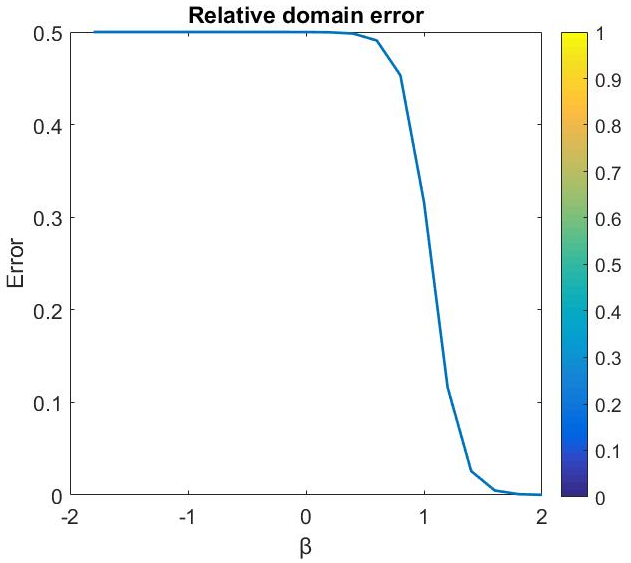

Figure 6.10: The domain error for different values of β for the decoupled model

6.2 Two-Dimensional Case

For the two-dimensional case we retain the same 2D geometry as used to study the one-dimensional case where we do no longer have no flow boundary conditions on the sides. The boundary conditions at the top of the domain is $p_1 = 0$, and at the bottom $p_2 = 1$. For the sides, the boundary conditions to the left is $p_3 = 0$ and to the right $p_4 = 1$. The problem is solved with the models described in the previous chapter for different values of α and β and compared to the reference solution.

For all the three upscaled models, we study the accuracy of this model for different values of α and β. In particular, we also study the validity of approximation outside the validity range of this model. We then show the error behaviour corresponding to different values of α and β. We refer to Section 4.3 for the summary of the upscaled models obtained for different values of α and β. Just to recall, we once again present the upscaled models here.

For the three cases, $\beta < 1, \beta = 1,$ and $\beta > 1$, we summarise the three upscaled models that we derived above. Interestingly, the 2D upscaled model also has the same structure. as the one-dimensional upscaled models.

1. Case 1: $\beta < 1$ **Average Model**

$$\frac{\partial^2 p_1}{\partial x^2} + \frac{\partial^2 p_1}{\partial y^2} = 0 \text{ in } \Omega_1, \tag{6.16}$$

$$\frac{\partial^2 p_2}{\partial x^2} + \frac{\partial^2 p_2}{\partial y^2} = 0 \text{ in } \Omega_2 \tag{6.17}$$

coupled through the interface conditions,

$$p_1 = p_2 \text{ at } \Gamma_1, \tag{6.18}$$

$$\frac{\partial p_1}{\partial y} = \frac{\partial p_2}{\partial y} \text{ at } \Gamma_1. \tag{6.19}$$

2. Case 2: $\beta = 1$ **Two-scale Model**
Define, $\Omega_\gamma = (-1, 1)$. The two-scale model is given by

$$\frac{\partial^2 p_1}{\partial x^2} + \frac{\partial^2 p_1}{\partial y^2} = 0 \text{ in } \Omega_1, \tag{6.20}$$

$$\frac{\partial^2 p_2}{\partial x^2} + \frac{\partial^2 p_2}{\partial y^2} = 0 \text{ in } \Omega_2, \tag{6.21}$$

$$\frac{\partial^2 p_f}{\partial x^2} + \frac{\partial^2 p_f}{\partial \gamma^2} = 0 \text{ in } \Omega_\gamma, \tag{6.22}$$

coupled through the interface conditions,

$$\begin{array}{l} \frac{\partial p_1}{\partial y}(y=1) = \frac{\partial p_f}{\partial \gamma} \quad \text{at } \gamma = -1 \\ \frac{\partial p_2}{\partial y}(y=1) = \frac{\partial p_f}{\partial \gamma} \quad \text{at } \gamma = 1 \end{array} \tag{6.23}$$

and

$$p_1(y=1) = p_f \quad \text{at } \gamma = -1 \tag{6.24}$$

and

$$p_2(y=1) = p_f \quad \text{at } \gamma = 1. \tag{6.25}$$

3. Case 3: $\beta > 1$ **Decoupled Model**

$$\frac{\partial^2 p_1}{\partial x^2} + \frac{\partial^2 p_1}{\partial y^2} = 0 \text{ in } \Omega_1, \tag{6.26}$$

$$\frac{\partial^2 p_2}{\partial x^2} + \frac{\partial^2 p_2}{\partial y^2} = 0 \text{ in } \Omega_2 \tag{6.27}$$

coupled through the interface conditions,

$$p_1 = p_2 \text{ at } \Gamma_1, \tag{6.28}$$

$$\frac{\partial p_1}{\partial y} = \frac{\partial p_2}{\partial y} \text{ at } \Gamma_1. \tag{6.29}$$

and decoupled at the interface by no flow boundary conditions,

$$\frac{\partial p_1}{\partial y} = \frac{\partial p_1}{\partial y} = 0 \text{ at } \Gamma_1. \tag{6.30}$$

In all these cases, we have used Dirichlet boundary conditions for pressure at $(0, y) = 0$, at $(2, y) = 1$, at $(x, 0) = 0$ and at $(x, 2) = 1$. These pressure boundary conditions are retained and remain unchanged for all the upscaled models.

6.2.1 The Average Model

1. We start with taking $\beta = 1$ and $\alpha = 1$ and compute the pressure profile using the Average Model, and the error with respect to the reference Epsilon model. We do no longer obtain a linear profile for pressure. See Figure 6.11.

2. We choose $\beta = 0$ and $\alpha = 0$ and solve both the full model, that is, the reference Epsilon model and the upscaled model. We compare the accuracy of the solution and behaviour of the error, and we then choose $\alpha = 2$ and $\beta = 0$ to see the effects of the vertical permeability (See Figure 6.2).

3. We choose a range of α and β values and show the behaviour of the error with respect to the reference Epsilon model (See Figure 6.12).

4. We finally locates the position of the error in Figure 6.13. Here $\alpha = 0$ and $\beta = 0$

Like in the one-dimensional case we expect this model to be working when there is an easy flow of information through the fracture in the y-direction. This happens when $\beta < 1$. This is tested in Figure 6.12 where the relative domain error is plotted for different values of α and β, and the figure shows that this model works as long as $\beta < 1$. From all the plots in Figure 6.11 and in from Figure 6.13 it becomes clear that the errors in this model is at its largest close to the fracture.

6.2.2 Conclusion

1. For the case where $\beta = 1$ and $\alpha = 1$ the pressure profile and the error with respect to the reference Epsilon model shows that the Average Model is no good approximation for this case. Note that the value of β and α is outside the validity range for this model. See Figure 6.11.

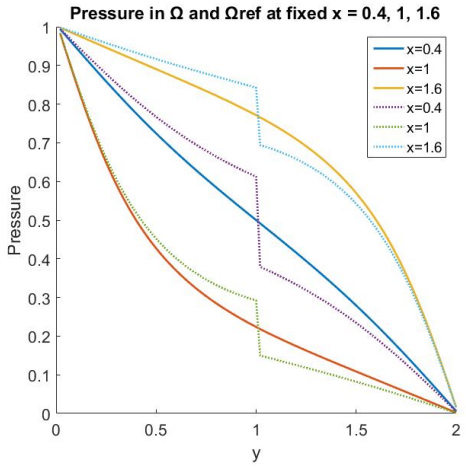

(a) Pressure for $\alpha = \beta = 1$.

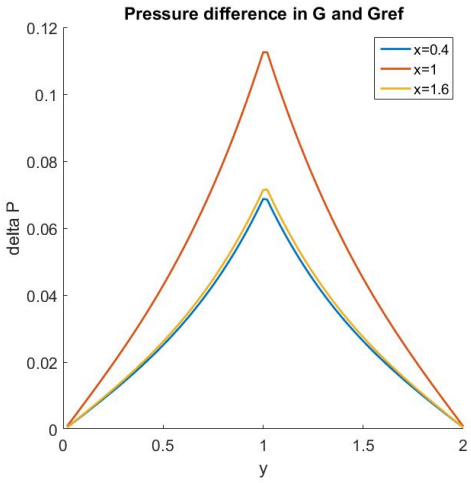

(b) Pressure difference between the average model and the reference model for $\alpha = \beta = 1$.

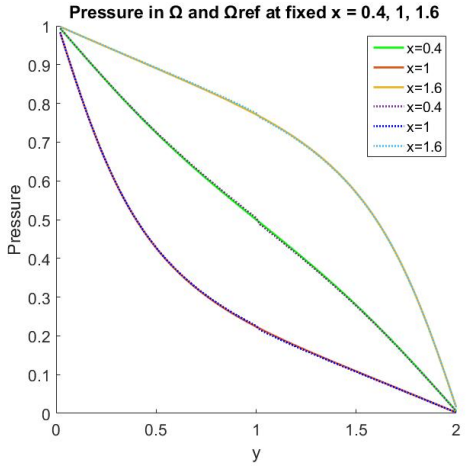

(c) Pressure for $\alpha = 0$ and $\beta = 0$.

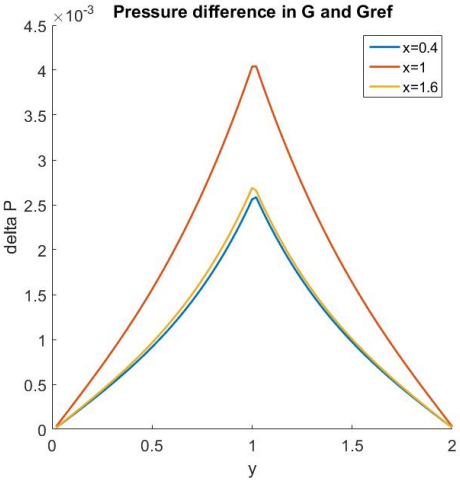

(d) Pressure difference between the average model and the reference model for $\alpha = 0$ and $\beta = 0$.

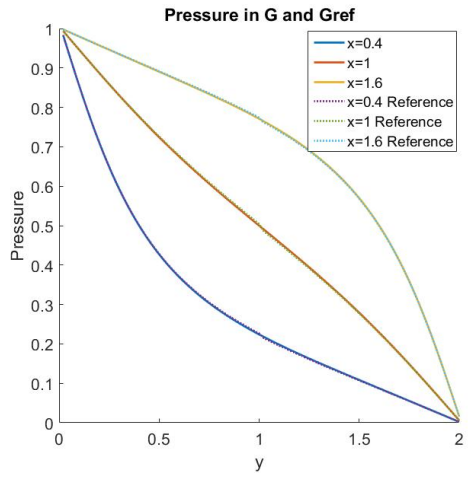

(e) Pressure for $\alpha = 2$ and $\beta = 0$.

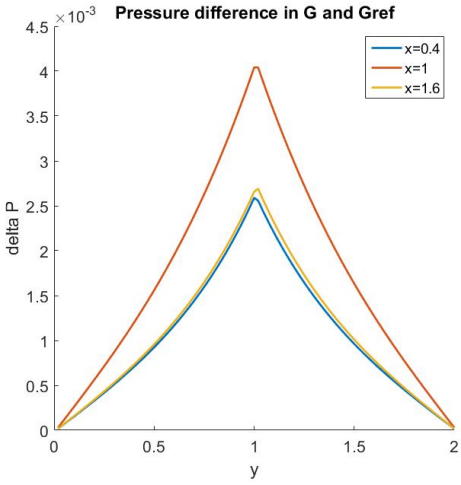

(f) Pressure difference between the average model and the reference model for $\alpha = 2$ and $\beta = 0$.

Figure 6.11: These figures shows the pressure plots at fixed x equal to 0.4, 1 and 1.8for different α and β values and the error in the different cases.

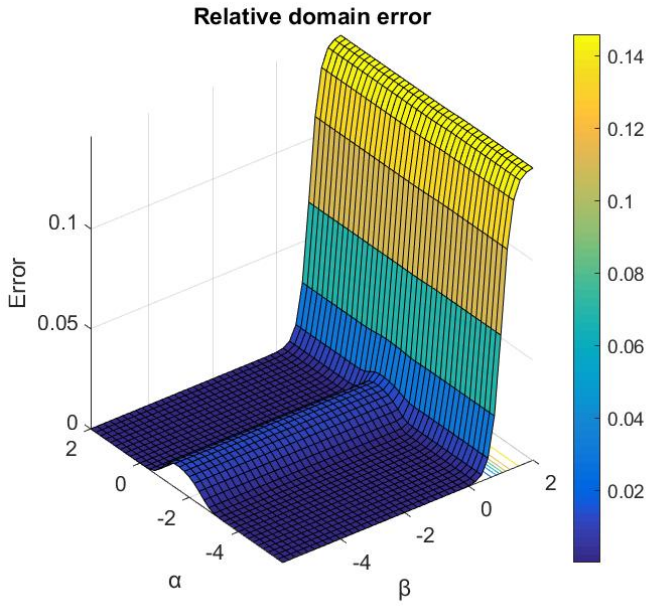

Figure 6.12: The relative domain error for different values of α and β for the average model in a two-dimensional domain.

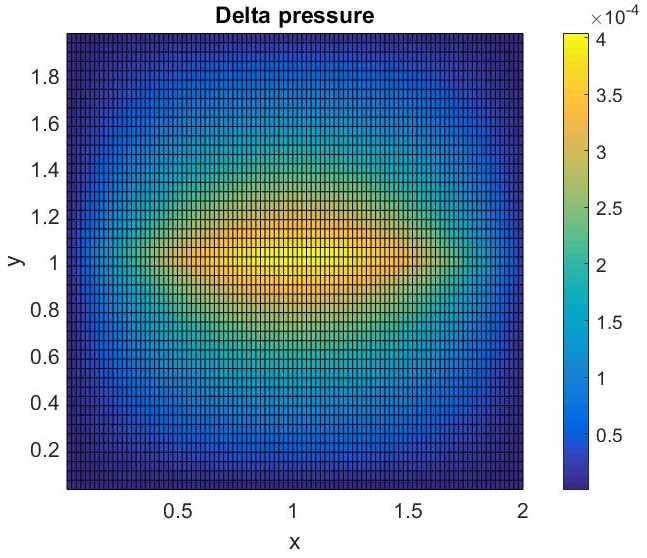

Figure 6.13: The error is plotted with respect to x and y to locate where the error occurs.

2. For $\beta = 0$ and variations in α we see that there is a good match between the reference Epsilon model and the upscaled model, and that the variation in α-value does not have an effect on the error for this particular case for $\beta = 0$. (See Figure 6.12).

3. We choose a range of α and β values and show the behaviour of the error with respect to the reference Epsilon model (See Figure 6.12). We observe that the Average model is validated for $\beta < 1$ and that the value of α does not play a significant role to validity of the Average Model

4. We finally locates the position of the error in Figure 6.13, and see that the error becomes larger closer to the fracture.

6.2.3 The Two Scale Model

1. We start with taking $\beta = 1$ and $\alpha = 1$ and solve the problem using the Two Scaled Model and the Epsilon Model. We find the error with respect to the reference Epsilon model (See Figure 6.14).

2. We choose $\beta = 1$ and $\alpha = -1$ and solve both the full model, that is, the reference Epsilon model and the upscaled model. We compare the accuracy of the solution and behaviour of the error (See Figure 6.14).

3. We choose $\beta = 1$ and $\alpha = 1.5$ and solve both the reference Epsilon model and the upscaled model. We compare the accuracy of the solution and behaviour of the error (See Figure 6.14).

4. We choose a range of α and β values and show the behaviour of the error with respect to the reference Epsilon model (See Figure 6.15).

5. We finally locates the position of the error in Figure 6.16. Here $\alpha = 1$ and $\beta = 1$

For a one-dimensional domain we have shown that this model works when the permeability in the y-direction is ϵ^1, which is when $\beta = 1$, but that does not necessary mean that the two scaled model will be a good approximation for a two-dimensional case. The permeability in the x-direction may play a significant role on the pressure distribution. In Figure 6.14a and Figure 6.14c the pressure is plotted for $\beta = 1$, but for different values of α. This does not seem to affect the epsilon model, but it has a great influence on the Two Scaled Model as shown in the errors plotted in Figure 6.14b and Figure 6.14d. The model does have some limitations with respect to α

6.2.4 Conclusion

1. For $\beta = 1$ and $\alpha = 1$ we find that the difference in the Two Scaled Model and the Epsilon Model is low. (See Figure 6.14).

2. For $\beta = 1$ and $\alpha = -1$ the reference Epsilon model and the upscaled model gives two different pressure profiles. There is a jump in the pressure for the Two Scaled Model while the Epsilon is almost continuous (See Figure 6.14).

3. For $\beta = 1$ and $\alpha = 1.5$ the difference in the two models is small. By changing α from -1 to 1.5 we reduce the difference between the Two Scaled Model and the Epsilon Model. The validity is dependent on α (See Figure 6.14).

4. We choose a range of α and β values and show the behaviour of the error with respect to the reference Epsilon model (See Figure 6.15). It becomes clear that the model is dependent on the α value as well as the β value.

5. The error location plotted in Figure 6.16 gives that the error occur close to the fracture. Here $\alpha = 1$ and $\beta = 1$

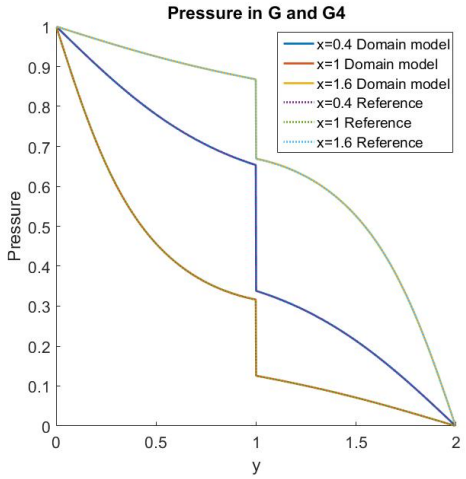

(a) Pressure for $\alpha = \beta = 1$.

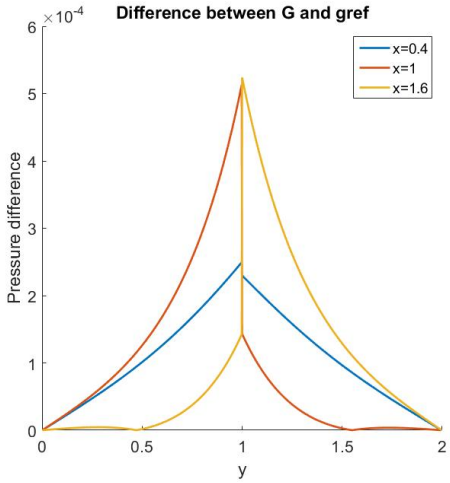

(b) Pressure difference between the two scaled model and the reference model for $\alpha = \beta = 1$.

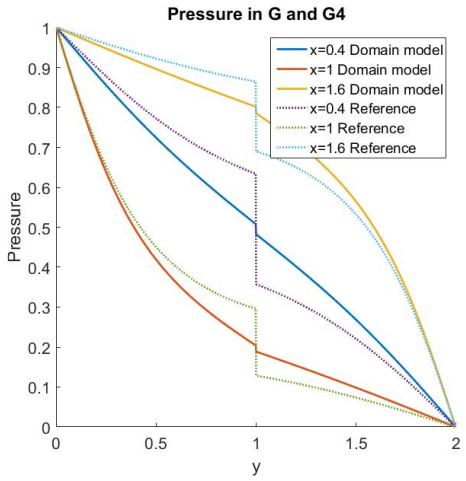

(c) Pressure for $\alpha = -1$ and $\beta = 1$.

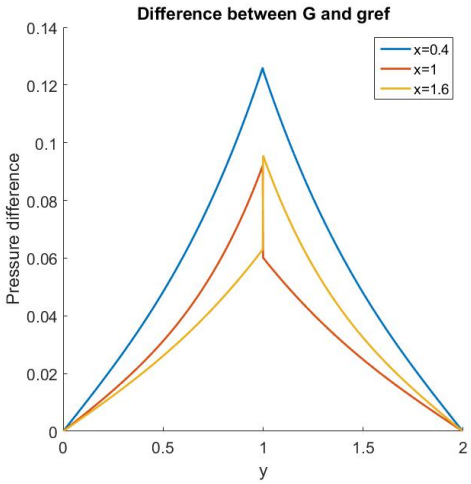

(d) Pressure difference between the two scaled model and the reference model for $\alpha = -1$ and $\beta = 1$.

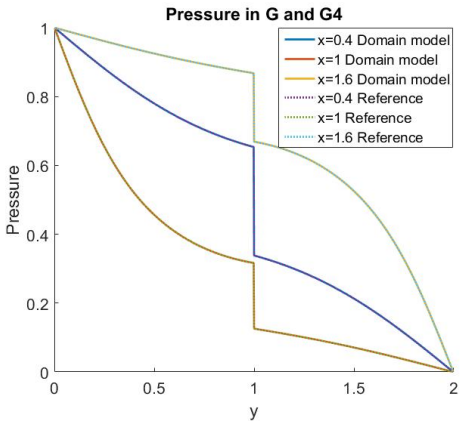

(e) Pressure when $\alpha = 1.5$ and $\beta = 1$.

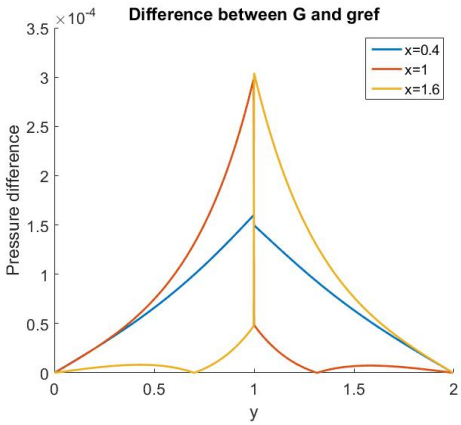

(f) Pressure difference between the two scaled model and the reference model for $\alpha = 1.5$ and $\beta = 1$.

Figure 6.14: The figures show the pressure profile at $x = 0.4$, 1 and 1.8 with respect to y for different values of α and β, and the pressure difference between the two scaled model and the reference model in the different cases.

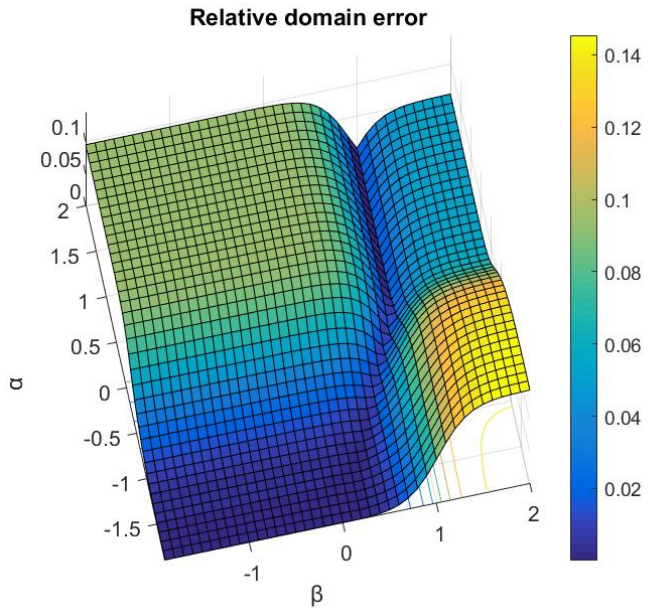

Figure 6.15: The domain error in the two scaled model for different values of α and β. The error is calculated with respect to the epsilon model using the euclidean norm.

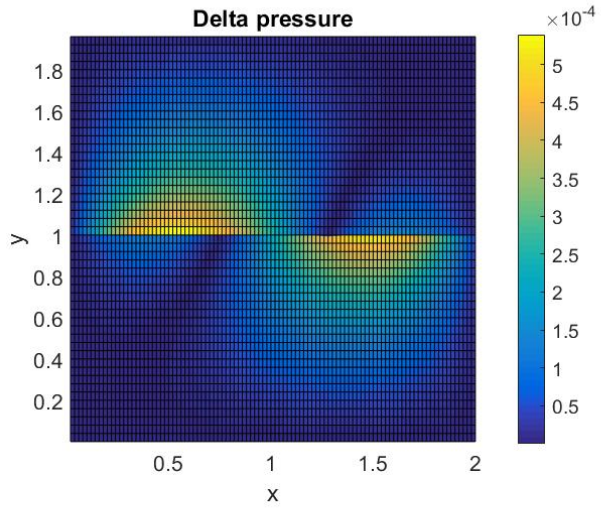

Figure 6.16: This plot shows the location of the error with respect to x and y. In this plot $\alpha = \beta = 1$.

6.2.5 The Decoupled Model

We consider the following cases:

1. We take $\alpha = \beta = 0$ and solve the model using the Decoupled Model and the Epsilon model. The decoupled profile is harder to see now that there are dirichlet boundary conditions on the sides of the domain. See Figure 6.1. For this case we are outside of the validity range of this model

2. We choose $\alpha = 1$ and $\beta = 1$ and solve both the full model, that is, the reference Epsilon model and the upscaled model. We compare the accuracy of the solution and behaviour of the error. (See Figure 6.17)

3. For $\alpha = \beta = 2$, we again compute both the reference solution and the Average model solution. We compare the error for this case. This value of β is inside the validity range of the upscaled model. (See Figure 6.2)

4. We choose a range of α and β values and show the behaviour of the error with respect to the reference Epsilon model (See Figure 6.18).

5. Finally we plot the pressure difference between the Decoupled model and the Epsilon model with respect to x and y to show the location of the error. This is done for $\alpha = \beta = 2$

This model is, like in the one-dimensional case, expected to be a good approximation when the permeability is greater than ϵ^1 in the y-direction. The relative domain error plotted in Figure 6.18 tells us that the Decoupled model is valid when $\beta > 1$, and it shows us that the α-value has little or no impact of the validity of this model.

6.2.6 Conclusion

1. For $\alpha = \beta = 0$ there is a gap between the Decoupled Model and the Epsilon model. This is as expected as this case is outside the validity range of $\beta > 1$ (See Figure 6.1).

2. For $\alpha = 1$ and $\beta = 1$ the Decoupled Model is a good approximation to the problem. The difference from the reference Epsilon model is small even though we expected this model to have validity for $\beta > 1$ (See Figure 6.17).

3. For $\alpha = \beta = 2$, we see that the Decoupled Model can be used as an good approximation to the problem. This value of β is inside the validity range of the upscaled model. (See Figure 6.2)

4. We choose a range of α and β values and show the behaviour of the error with respect to the reference Epsilon model (See Figure 6.18). We observe that the approximation quality of this model increases as the value of β increases. The error increases fast especially outside the validity range. This provides a good agreement with the quality of the upscaling improving as we increase β

5. The plot of the pressure difference between the Decoupled model and the Epsilon gives us that the error is located close to the fracture.

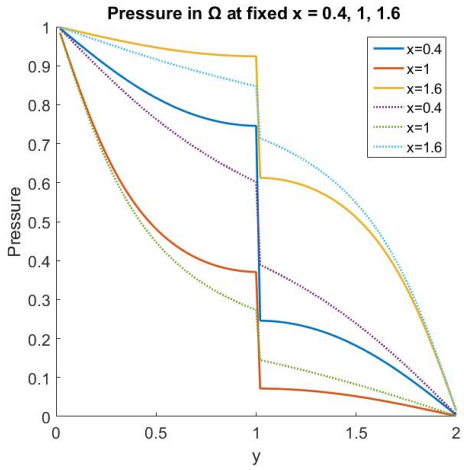

(a) Pressure profile for $\alpha = \beta = 0$.

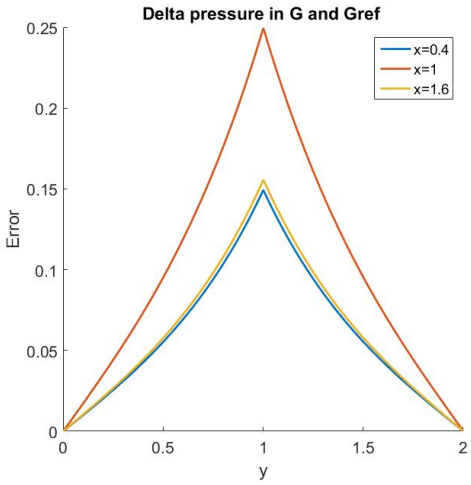

(b) Pressure difference between the decoupled model and the reference model for $\alpha = \beta = 0$.

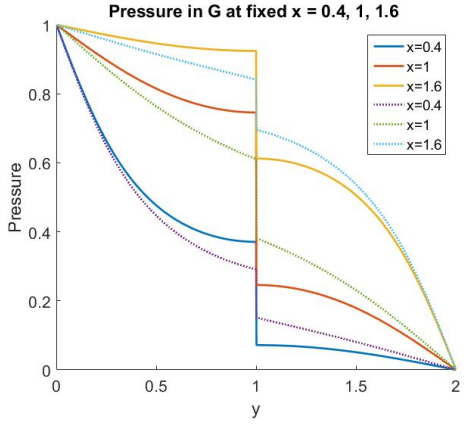

(c) Pressure profile for $\alpha = 1$ and $\beta = 1$.

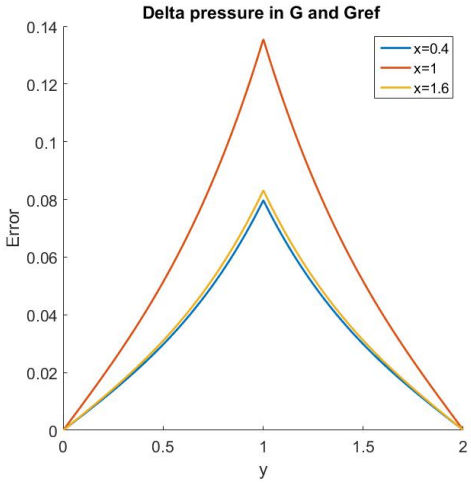

(d) Pressure difference between the decoupled model and the reference model for $\alpha = 1$ and $\beta = 1$.

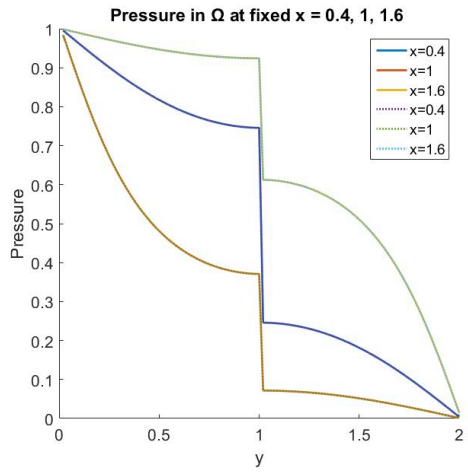

(e) Pressure profile for $\alpha = 2$ and $\beta = 2$.

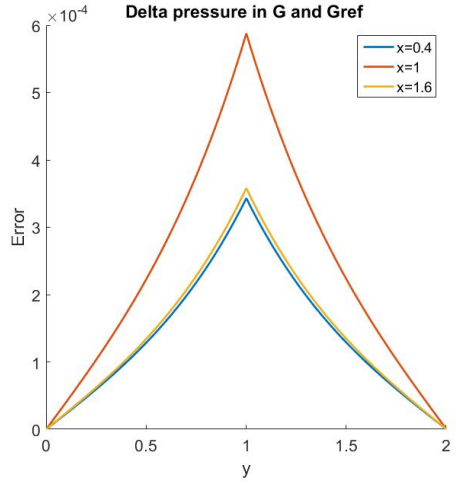

(f) Pressure difference between the decoupled model and the reference model for $\alpha = 2$ and $\beta = 2$.

Figure 6.17: The pressure profiles and the pressure differences for the decoupled model are ploted for $x = 0.4,\ 1$, and 1.8 for different values of α and β.

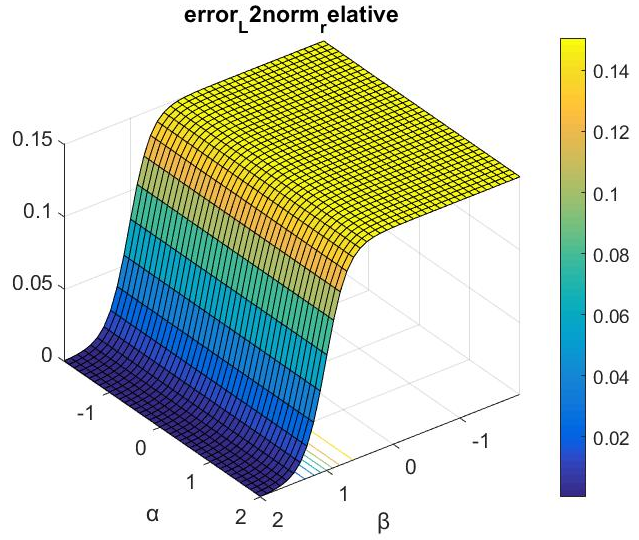

Figure 6.18: The domain error in the decoupled model. The error is calculated with respect to the epsilon model for different values of α and β using the euclidean norm

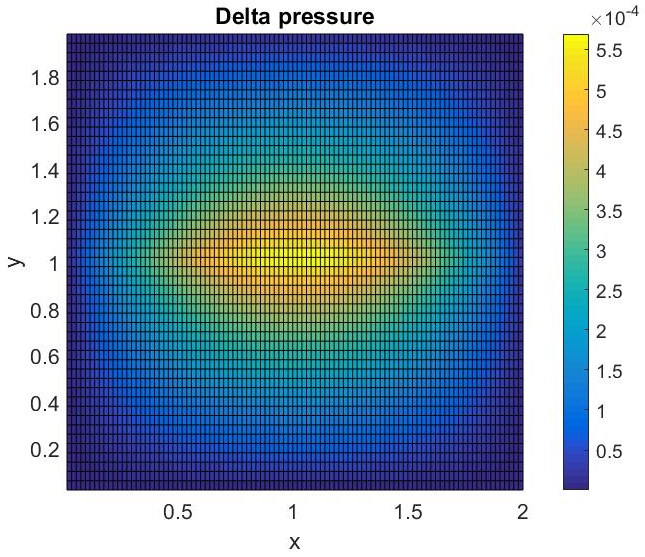

Figure 6.19: This figure shows where the error is located with respect to x and y for $\alpha = \beta = 2$

Chapter 7

Conclusion

Throughout this thesis we have rigorously derived upscaled models for fractured flow as the size of the fracture $\epsilon \to 0$. This has been studied by scaling the permeability as an exponent of the width of the fracture, and we have studied the quality of the models for different exponential values α and β. We have derived a weak formulation and an analytical solution of a dual problem in one-dimension to estimate the flux in a fracture, and investigated numerical computations for the upscaled model. Our numerical computations in two-dimension reveal that in the absence of periodic boundary conditions, the flow profile inside the fracture may become quite complex.

Detailed observations concerning the quality of upscaling have been discussed in Chapter 6. We point out some of the general observations here. We observe that the upscaled models approximate the reference solution quite well within the validity range of α, β, the parameters that characterise the permeability of the fracture. Moreover, we see that the approximation is quite poor when the parameter values are outside the validity range. This underlines the central point of this thesis that the upscaled models need to be derived corresponding to the parameter range we have in a particular problem. Finally, we note that the boundary conditions on the lateral sides of the fracture influence the upscaling quality. We also see that both α and β influence the error behaviour for any particular choice of upscaled model.

7.1 Further work

The thesis considers the simplest model available for studying the upscaling of fracture flow. Several extensions of this study can profitably use the techniques and insights developed in this thesis. In particular, we point out the following extensions of this work that need to be considered and left for future studies.

1. The 2D problem has not yet been completed in full detail. Whereas we have pointed out certain structure of the upscaled model and performed numerical computations, a complete study of this model remains unaccomplished. In particular, for the cases when α and β influence the upscaled model in the case when the boundary conditions are not periodic in the lateral direction. Also, the Dual problem approach that we have developed here remains incomplete in the case when $\beta < 1$. For this case, the energy methods work whereas we have not been able to complete the arguments using the Dual problem approach. Moreover, certain arguments for 2D case are still heuristic though they can be made rigorous by employing abstract mathematical ideas that are outside the scope of this thesis.

2. In terms of the models, we have only considered the simplest model. Several extensions are due. To begin with, we can extend the results to the parabolic case. A linear heat equation, for example, can be dealt with the results derived in this work without much

difficulty. However, what remains incomplete is any extension to non-linearity or including further models. For instance, these results should be extended to the case of a reactive transport such as described by (Pop, Bogers, & Kumar, 2016; Kumar, Pop, & Radu, 2014, 2013).

3. In terms of geometry, we have again considered the simplest geometrical shape. These results should be extended to the case when the fracture surface is non-planar. This would require defining the surface derivatives and concepts from differential geometry. Moreover, extending the problem to work for a three-dimensional problem for a planar fracture can be performed using the arguments here for certain cases. However, a full 3D problem even in the case of planar fracture remains unresolved.

4. As previously mentioned, the extension to more complex models such as multiphase flow and numerical methods to solve them (see e.g., (F. A. Radu, Nordbotten, Pop, & Kumar, 2015; F. Radu, Pop, & Knabner, 2004; Pop, Radu, & Knabner, 2004; F. A. Radu, Pop, & Knabner, 2008; F. A. Radu, Pop, & Attinger, 2010)) will require more advanced techniques than the ones in this thesis.

References

Adler, P. M., Thovert, J.-F., & Mourzenko, V. V. (2012). *Fractured porous media.* Oxford University Press.

Alboin, C., Jaffré, J., Roberts, J. E., & Serres, C. (2002). Modeling fractures as interfaces for flow and transport. In *Fluid flow and transport in porous media, mathematical and numerical treatment: Proceedings of an ams-ims-siam joint summer research conference on fluid flow and transport in porous media, mathematical and numerical treatment, june 17-21, 2001, mount holyoke college, south hadley, massachusetts* (Vol. 295, p. 13).

Anderson, J. D., & Wendt, J. (1995). *Computational fluid dynamics* (Vol. 206). Springer.

Barenblatt, G., Zheltov, I. P., & Kochina, I. (1960). Basic concepts in the theory of seepage of homogeneous liquids in fissured rocks [strata]. *Journal of applied mathematics and mechanics*, *24*(5), 1286–1303.

Bastian, P., Chen, Z., Ewing, R. E., Helmig, R., Jakobs, H., & Reichenberger, V. (2000). Numerical simulation of multiphase flow in fractured porous media. In Z. Chen, R. E. Ewing, & Z.-C. Shi (Eds.), *Numerical treatment of multiphase flows in porous media: Proceedings of the international workshop held a beijing, china, 2–6 august 1999* (pp. 50–68). Berlin, Heidelberg: Springer Berlin Heidelberg.

Bear, J. (1988). *Dynamics of fluids in porous media.* Dover Publications, INC.

Berkowitz, B., Bear, J., & Braester, C. (1988). Continuum models for contaminant transport in fractured porous formations. *Water Resources Research*, *24*(8), 1225–1236.

Bukač, M., Yotov, I., & Zunino, P. (2015). An operator splitting approach for the interaction between a fluid and a multilayered poroelastic structure. *Numerical Methods for Partial Differential Equations*, *31*(4), 1054–1100.

Bukac, M., Yotov, I., & Zunino, P. (2016). Dimensional model reduction for flow through fractures in poroelastic media. *ESAIM: Mathematical Modelling and Numerical Analysis*.

Chen, X., Pond, C., & Wang, X. (2012). Effective boundary conditions resulting from anisotropic and optimally aligned coatings: the two dimensional case. *Archive for Rational Mechanics and Analysis*, 1–41.

Dietrich, P., Helmig, R., Sauter, M., Hötzl, H., Köngeter, J., & Teutsch, G. (2005). *Flow and transport in fractured porous media.* Springer Science & Business Media.

Formaggia, L., Fumagalli, A., Scotti, A., & Ruffo, P. (2014). A reduced model for darcys problem

in networks of fractures. *ESAIM: Mathematical Modelling and Numerical Analysis*, *48*(4), 1089–1116.

Fumagalli, A., & Scotti, A. (2013). A numerical method for two-phase flow in fractured porous media with non-matching grids. *Advances in Water Resources*, *62*, 454–464.

Gerke, H., & Genuchten, M. V. (1993). A dual-porosity model for simulating the preferential movement of water and solutes in structured porous media. *Water resources research*, *29*(2), 305–319.

Girault, V., Kumar, K., & Wheeler, M. F. (2016). Convergence of iterative coupling of geomechanics with flow in a fractured poroelastic medium. *Computational Geosciences*, *20*(5), 997–1011.

Gong, B., Karimi-Fard, M., Durlofsky, L. J., et al. (2008). Upscaling discrete fracture characterizations to dual-porosity, dual-permeability models for efficient simulation of flow with strong gravitational effects. *SPE Journal*, *13*(01), 58–67.

Gudmundsson, A., Løtveit, I. F., & Gjesdal, O. (2002). Fracture-generated permeability and groundwater yield in norway.

Hægland, H., Assteerawatt, A., Dahle, H. K., Eigestad, G. T., & Helmig, R. (2009). Comparison of cell-and vertex-centered discretization methods for flow in a two-dimensional discrete-fracture–matrix system. *Advances in water resources*, *32*(12), 1740–1755.

Helmig, R., et al. (1997). *Multiphase flow and transport processes in the subsurface: a contribution to the modeling of hydrosystems.* Springer-Verlag.

Hill, A., Thomas, G., et al. (1985). A new approach for simulating complex fractured reservoirs. In *Middle east oil technical conference and exhibition.*

Kazemi, H., et al. (1969). Pressure transient analysis of naturally fractured reservoirs with uniform fracture distribution. *Society of petroleum engineers Journal*, *9*(04), 451–462.

Kincaid, D. R., & Cheney, E. W. (2002). *Numerical analysis: mathematics of scientific computing* (Vol. 2). American Mathematical Soc.

Kumar, K., Neuss-Radu, M., & Pop, I. S. (2016). Homogenization of a pore scale model for precipitation and dissolution in porous media. *IMA Journal of Applied Mathematics*, *81*(5), 877–897.

Kumar, K., Pop, I. S., & Radu, F. (2014). Convergence analysis for a conformal discretization of a model for precipitation and dissolution in porous media. *Numerische Mathematik*, *127*(4), 715–749.

Kumar, K., Pop, I. S., & Radu, F. A. (2013). Convergence analysis of mixed numerical schemes for reactive flow in a porous medium. *SIAM Journal on Numerical Analysis*, *51*(4), 2283–2308.

Kumar, K., Van Noorden, T., & Pop, I. S. (2011). Effective dispersion equations for reactive flows involving free boundaries at the microscale. *Multiscale Modeling & Simulation*, *9*(1),

29–58.

Kumar, K., van Noorden, T., & Pop, I. S. (2014). Upscaling of reactive flows in domains with moving oscillating boundaries. *Discrete Contin. Dyn. Sys. Ser. S*, *7*, 95–111.

Kundu, P. K., Cohen, I. M., & Dowling, D. R. (2012). *Fluid mechanics*. Elsevier.

Lie, K.-A. (2015). An introduction to reservoir simulation using matlab user guide for the matlab reservoir simulation toolbox (mrst). In (Vol. 303). SINTEF ICT, Departement of Applied Mathematics Oslo, Norway.

Lie, K.-A., Krogstad, S., Ligaarden, I. S., Natvig, J. R., Nilsen, H. M., & Skaflestad, B. (2012). Open-source matlab implementation of consistent discretisations on complex grids. *Computational Geosciences*, *16*(2), 297–322.

Lien, J. (2004). *Ptek211 grunnleggende reservoarfyskk (kjeneranalyse og logging)*. Bergen, Universitetet i Bergen-Institutt for fysikk og teknologi.

Martin, V., Jaffré, J., & Roberts, J. E. (2005). Modeling fractures and barriers as interfaces for flow in porous media. *SIAM Journal on Scientific Computing*, *26*(5), 1667–1691.

Neuss-Radu, M., & Jäger, W. (2007). Effective transmission conditions for reaction-diffusion processes in domains separated by an interface. *SIAM Journal on Mathematical Analysis*, *39*(3), 687–720.

Nield, D. A., & Bejan, A. (2006). *Convection in porous media*. Springer Science & Business Media.

Nordbotten, J. M., & Celia, M. A. (2012). *Geological storage of co_2*. Hoboken, Wiley.

Onsager, L. (1931). Reciprocal relations in irreversible processes. i. *Physical review*, *37*(4), 405.

Pop, I. S., Bogers, J., & Kumar, K. (2016). Analysis and upscaling of a reactive transport model in fractured porous media with nonlinear transmission condition. *Vietnam Journal of Mathematics*, 1–26.

Pop, I. S., Radu, F., & Knabner, P. (2004). Mixed finite elements for the richards equation: linearization procedure. *Journal of computational and applied mathematics*, *168*(1), 365–373.

Pruess, K., et al. (1985). A practical method for modeling fluid and heat flow in fractured porous media. *Society of Petroleum Engineers Journal*, *25*(01), 14–26.

Radu, F., Pop, I. S., & Knabner, P. (2004). Order of convergence estimates for an euler implicit, mixed finite element discretization of richards' equation. *SIAM Journal on Numerical Analysis*, *42*(4), 1452–1478.

Radu, F. A., Nordbotten, J. M., Pop, I. S., & Kumar, K. (2015). A robust linearization scheme for finite volume based discretizations for simulation of two-phase flow in porous media. *Journal of Computational and Applied Mathematics*, *289*, 134–141.

Radu, F. A., Pop, I. S., & Attinger, S. (2010). Analysis of an euler implicit-mixed finite element scheme for reactive solute transport in porous media. *Numerical Methods for Partial Differential Equations*, *26*(2), 320–344.

Radu, F. A., Pop, I. S., & Knabner, P. (2008). Error estimates for a mixed finite element discretization of some degenerate parabolic equations. *Numerische Mathematik*, *109*(2), 285–311.

Reichenberger, V., Jakobs, H., Bastian, P., & Helmig, R. (2006). A mixed-dimensional finite volume method for two-phase flow in fractured porous media. *Advances in Water Resources*, *29*(7), 1020–1036.

Samardzioska, T., & Popov, V. (2005). Numerical comparison of the equivalent continuum, non-homogeneous and dual porosity models for flow and transport in fractured porous media. *Advances in water resources*, *28*(3), 235–255.

Singh, G., Pencheva, G., Kumar, K., Wick, T., Ganis, B., Wheeler, M. F., et al. (2014). Impact of accurate fractured reservoir flow modeling on recovery predictions. In *Spe hydraulic fracturing technology conference.*

Tanaka, N., Ninokata, H., & Wada, A. (2002). *Advances in fluid modeling & turbulence measurements: Proceedings of the 8th international symposium on flow modeling and turbulence measurements: Tokyo, japan, 4-6 december 2001.* World Scientific.

TUNC, X. (2012). *La modlisation des failles conductrices pour les coulements en milieux poreux* (Unpublished doctoral dissertation). UNIVERSIT DE PROVENCE.

Warren, J., Root, P. J., et al. (1963). The behavior of naturally fractured reservoirs. *Society of Petroleum Engineers Journal*, *3*(03), 245–255.

Witherspoon, P. A., Wang, J. S., Iwai, K., & Gale, J. E. (1980). Validity of cubic law for fluid flow in a deformable rock fracture. *Water resources research*, *16*(6), 1016–1024.

Zolotukhin, A. B., & Ursin, J.-R. (2000). *Introduction to petroleum reservoir enginering.* Høyskoleforlaget AS.